

1 **On the field estimation of moisture content using**
2 **electrical geophysics—the impact of petrophysical**
3 **model uncertainty**

4 **Chak-Hau Michael Tso^{1,3}, Oliver Kuras², and Andrew Binley¹**

5 ¹Lancaster Environment Centre, Lancaster University

6 ²British Geological Survey

7 ³Now at Centre for Ecology and Hydrology

8
9 ¹Library Avenue, Lancaster, LA1 4YQ, United Kingdom

10 ²Environmental Science Centre, Keyworth, Nottingham NG12 5GG, United Kingdom

11 ³Library Avenue, Lancaster, Lancaster LA1 4AP, UK

12 **Key Points:**

- 13 • Field evidence demonstrating strong variability of petrophysical relationships at
14 the site
- 15 • The proposed methods show the impact of different uncertain $\theta(\rho)$ models on θ
16 estimates from ERT and their associated uncertainty bounds
- 17 • Nevertheless, different Archie models give consistent difference in θ estimates, though
18 their uncertainty bounds are large

This article has been accepted for publication and undergone full peer review but has not been through the copyediting, typesetting, pagination and proofreading process which may lead to differences between this version and the Version of Record. Please cite this article as doi: 10.1029/2019WR024964

Corresponding author: Michael Tso, m.tso@lancaster.ac.uk, mtso@ceh.ac.uk

Abstract

The spatiotemporal distribution of pore water in the vadose zone can have a critical control on many processes in the near-surface Earth, such as the onset of landslides, crop yield, groundwater recharge, and runoff generation. Electrical geophysics has been widely used to monitor the moisture content (θ) distribution in the vadose zone at field sites, and often resistivity (ρ) or conductivity (σ) is converted to moisture contents through petrophysical relationships (e.g. Archie's law). Though both the petrophysical relationships (i.e. choices of appropriate model and parameterisation) and the derived moisture content are known to be subject to uncertainty, they are commonly treated as exact and error-free. This study examines the impact of uncertain petrophysical relationships on the moisture content estimates derived from electrical geophysics. We show from a collection of data from multiple core samples that significant variability in the $\theta(\rho)$ relationship can exist. Using rules of error propagation, we demonstrate the combined effect of inversion and uncertain petrophysical parameterization on moisture content estimates and derive their uncertainty bounds. Through investigation of a water injection experiment, we observe that the petrophysical uncertainty yields a large range of estimated total moisture volume within the water plume. The estimates of changes in water volume, however, generally agree within (large) uncertainty bounds. Our results caution against solely relying on electrical geophysics to estimate moisture content in the field. The uncertainty propagation approach is transferrable to other field studies of moisture content estimation.

Plain language summary

Maps and images of electrical resistivity have been widely applied to effectively monitor the wetting or drying of the Earth's near-surface. But how well can they quantify such change? How variable are the petrophysical model parameters that relate resistivity and moisture content? Does uncertainty in such relationships impact our confidence in moisture content estimates from resistivity imaging? Our analysis of field samples collected at a UK field site reveals great variability in petrophysical parameters. Using an uncertainty propagation method, which combines the uncertainty contributions from both petrophysical parameters and resistivity data errors, we find that the variable petrophysical parameters can lead to high uncertainty in moisture content estimates and they appear to be the dominating factor in many cases. These effects on uncertainty are greater than previously appreciated. The implication is that realistic uncertainty bounds are needed whenever electrical geophysical methods are used to quantify the amount of water present underground or its changes over time. The findings highlight the importance of better characterization of petrophysical parameters and the need to supplement the interpretation of resistivity-based moisture content estimates with other data sources.

1 Introduction

Monitoring the amount of moisture in the Earth's near-surface is critical in many applications. For example, the distribution of soil moisture is an important trigger for landslides (Ray & Jacobs, 2007). The amount of water available for root water uptake is the most important factor for crop yield (Ahmed, Passioura, & Carminati, 2018). Similarly, the saturation of the vadose zone governs the rate of groundwater recharge and travel times of surface contaminants (e.g. nitrate) to an aquifer (Green et al., 2018; Turkeltaub, Jia, Zhu, Shao, & Binley, 2018).

The measurement of moisture content (θ) in the subsurface is not straightforward. Point sampling can only cover a small number of discrete points in an investigation area and can be labour intensive. These point data may not be representative of site-scale variability. In addition, intrusive sampling may disrupt the critical processes occurring in the soil (e.g. root growth). Alternative field methods are needed to improve our ability to measure and monitor moisture content. A comprehensive review of the different ground-based methods to determine soil moisture is given by Jonard et al. (2018).

The well-established correlation between moisture content and the bulk resistivity (ρ) in porous media (Glover, 2015; Lesmes & Friedman, 2005) allows the use of electrical methods (e.g. electrical resistivity tomography (ERT) and electromagnetic induction (EMI)) to be applied to study vadose zone processes. They can be used to derive 2-D or 3-D distributed resistivity models over a relatively large area and these resistivity models can, in turn, be used for translation to moisture content via petrophysical relationships. ERT or EMI offers much larger spatial coverage than point-based methods without disrupting the Earth materials. Specifically, ERT is typically performed in transects or between boreholes, while EMI tends to provide even greater spatial coverage since it is commonly used for mapping. When applied in time-lapse mode, they can be a powerful tool to reveal temporal variations in soil moisture (Robinson et al., 2009).

Over the past two decades, electrical geophysics has been widely used in many applications in the vadose zone and increasingly the resistivity images are translated to obtain quantitative estimates of moisture content. Examples of these applications include monitoring the onset of landslides (Lehmann et al., 2013; Uhlemann et al., 2017), hill-slope moisture dynamics (Bass, Cardenas, & Befus, 2017; Cassiani et al., 2009; Hübner, Heller, Günther, & Kleber, 2015; Yamakawa, Kosugi, Katsura, Masaoka, & Mizuyama, 2012), seasonal changes in soil moisture dynamics (Amidu & Dunbar, 2007; Binley, Winship, West, Pokar, & Middleton, 2002), root zone water uptake (Beff, Günther, Vandoorne, Couvreur, & Javaux, 2013; Brillante, Mathieu, Bois, Van Leeuwen, & Lévêque, 2015; Garré, Javaux, Vanderborcht, Pagès, & Vereecken, 2011), unfrozen moisture in permafrost (Oldenborger & LeBlanc, 2015), soil moisture profiles beneath different wheat genotypes (Shanahan, Binley, Whalley, & Watts, 2015), watershed characterization (Miller, Routh, Brosten, & McNamara, 2008), and wetland dynamics (Chambers et al., 2014; Scaini et al., 2017; Uhlemann et al., 2016). Previous laboratory studies have shown that ERT is suitable for characterizing moisture content dynamics and tracer breakthrough in the unsaturated zone (e.g. Koestel, Kemna, Javaux, Binley, & Vereecken, 2008; Wehrer & Slater, 2015).

To translate resistivities to moisture content, a petrophysical relationship needs to be determined. (Note that although the root "petro" implies an application related to rocks (as in this study), similar physical laws applies to soils as well.) One common method is to take core samples from the field for laboratory testing (Amidu & Dunbar, 2007) using well-established procedures (see Hen-Jones et al., 2017; Jayawickreme, van Dam, & Hyndman, 2008). The samples are often oven dried and re-wetted and their resistivities are then repeatedly measured as their saturation changes. Although hysteresis has been reported in the wetting-drying behaviour of samples, laboratory testing is usually only applied to a single drying or wetting regime. Another method is to calibrate field-based inverted resistivity from ERT with in-situ measurements of soil moisture, for example

108 using time-domain reflectometry (TDR) probes. Several studies have compared mois-
109 ture content estimates from TDR and ERT (Brunet, Clément, & Bouvier, 2010) and in
110 recent years it has become increasingly popular to use such field-derived petrophysical
111 relationships. The local TDR-derived moisture content is taken as error-free and this is
112 typically used to calibrate against inverted resistivities using Archie's, Waxman-Smiths
113 (Cassiani et al., 2009; Garré et al., 2013; Lehmann et al., 2013; Michot et al., 2003), or
114 data-driven models (Brillante et al., 2014). More recently, calibration methods have been
115 developed for apparent electrical conductivity (ECa) from EMI against TDR-derived mois-
116 ture content (Robinet et al., 2018). The repeated EMI-moisture content monitoring study
117 of Martini et al. (2017) shows that this is not as straightforward as the relationship be-
118 tween electrical conductivity and moisture content can change with time. Whalley et al.
119 (2017) compared the change in electrical conductivity from EMI and ERT with changes
120 in water content from neutron probe measurements. The third (and perhaps most com-
121 mon) option is to simply use literature values for petrophysical parameters (e.g. Fried-
122 man, 2005). Regardless of the method for the assignment of petrophysical relationships,
123 errors will be present in some form. Laboratory measurements assume the observed re-
124 lationship and errors from small samples taken at a few locations can be applied to the
125 entire resistivity model. Field-based petrophysical relationships, on the other hand, as-
126 sume the inverted resistivity model having insignificant and uncorrelated errors so that
127 they can be used to calibrate against in-situ soil moisture data. In other words, the re-
128 sistivity model uncertainty is implicitly counted twice.

129 The uncertainty of the moisture content estimates from electrical geophysics stems
130 not only from the uncertainty in the resistivity model, but it also propagates through
131 from any constitutive relationships linking geophysical and hydrological properties, and
132 yet these relationships are frequently assumed to be precise and error-free (Binley et al.,
133 2015), in part due to the time and effort required to measure petrophysical parameters
134 in the lab. In fact, they are known to be uncertain due to the competing properties of
135 the pore fluids, pore geometry, and pore surface area on resistivity measurements (Weller,
136 Slater, & Nordsiek, 2013). Petrophysical model uncertainty is also one of the primary
137 factors limiting the utility of coupled inversion approaches (i.e. joint estimation of geo-
138 physical and hydraulic properties) (Singha, Day-Lewis, Johnson, & Slater, 2014). While
139 some stochastic modelling approaches (Hermans, Nguyen, & Caers, 2015; Hinnell et al.,
140 2010; Wiese, Wagner, Norden, Maurer, & Schmidt-Hattenberger, 2018, e.g.) allow some
141 modifications so that petrophysical model uncertainty can be accounted for, resolving
142 issues caused by such uncertainty remains an area of research. Recent coupled inversion
143 approaches allow the option to jointly estimate petrophysical parameters. Kuhl, Kendall,
144 Van Dam, and Hyndman (2018) devised a coupled inversion approach to jointly estimate
145 soil hydraulic parameters, petrophysical parameters and root parameters simultaneously.
146 Such methods are promising but there are concerns over the non-uniqueness in the in-
147 verse problem formulation and that the petrophysical parameters obtained may merely
148 be "effective" ones. In summary, research is needed to investigate the extent of the im-
149 pact on moisture content estimates due to uncertain petrophysical relationships.

150 The oil and gas industry, from where many of the foundational petrophysical re-
151 lationships used in hydrogeophysics are borrowed, or originate, has been aware of the
152 potential impact of petrophysical uncertainty. For example, Glover (2017) highlighted
153 that various sources of uncertainties in Archie parameters can lead to 20-40% error in
154 hydrocarbon saturation. For instance, even an uncertainty of 0.01 in a saturation expo-
155 nent of 2 (i.e. 0.5% or 2 ± 0.01) would result in an error in global oil reserves of about
156 USD \pm 254.36 billion based on figures in December 2015. While it is difficult to put
157 a monetary value on many near-surface applications, the above calculation underscores
158 the highly sensitive nature of petrophysical parameters and one should anticipate a sim-
159 ilar scale of error in soil water content estimation from electrical hydrogeophysics.

160 It is not until recently that the issues associated with petrophysical uncertainty have
161 been investigated. The pioneering work of Brunetti, Linde, and Vrugt (2017) considered
162 the effect of petrophysical uncertainty on using ground penetrating radar (GPR) data
163 for Bayesian hydrological model selection. There has also been some study on the pa-
164 rameter uncertainty of petrophysical models. For instance, Laloy, Javaux, Vanclooster,
165 Roisin, and Bielders (2011) tested five ‘pedo-electrical’ models for the reproduction of
166 electrical resistivity (determined by ERT) in a silt loam soil sample across a range of mois-
167 ture and bulk density values. They were inverted within a Bayesian framework, thereby
168 identifying not only the optimal parameter set but also parameter uncertainty and its
169 effect on model prediction. However, to date, there has not been any study on how the
170 uncertainty of petrophysical relationships affects the quantitative estimation of soil wa-
171 ter in the vadose zone using electrical geophysics. The findings on this question are rel-
172 evant to many applications mentioned above.

173 In this work, we present a first attempt to investigate the extent to which mois-
174 ture content estimates are affected by uncertainty in petrophysical models. Our aims are
175 to understand the likely variability in petrophysical models, and to develop a method
176 for petrophysical uncertainty propagation, which can be used to explore contributions
177 to uncertainty in the estimation of soil moisture. We review time-lapse ERT monitor-
178 ing data of a controlled infiltration experiment and the rock core data collected in the
179 same formation. We test the two types of petrophysical models on the core data and ap-
180 ply it to the inverted resistivity model, while keeping track of the uncertainty propaga-
181 tion quantitatively. The methods and data used in this work are detailed in section 2.
182 We report results from our analysis in section 3. Finally, we discuss our findings in sec-
183 tion 4 and provide our conclusions in section 5.

34 2 Materials and methods

185 Our study focuses on data from earlier comprehensive field and laboratory inves-
186 tations, at Hatfield (near Doncaster, South Yorkshire, UK) and Eggborough (near Selby,
187 North Yorkshire, UK). Two field sites, 17 km apart from each other, were instrumented
188 to study recharge processes to a Sherwood Sandstone aquifer. Tracer injection exper-
189 iments, monitored by both ERT and ground penetrating radar (GPR), were performed
190 at both sites. At Eggborough, ERT and GPR surveys were conducted in 1999 (Binley,
191 Cassiani, Middleton, & Winship, 2002; Cassiani & Binley, 2005) and the data were used
192 to study the utility of joint inversion of ERT and GPR data (Bouchedda, Chouteau, Bin-
193 ley, & Giroux, 2012; Linde, Binley, Tryggvason, Pedersen, & Revil, 2006) and the influ-
195 ence of prior information on vadose zone parameters estimation in stochastic inversion
196 (Scholer, Irving, Binley, & Holliger, 2011). Similarly, both ERT and GPR surveys were
197 conducted during tracer injection at Hatfield and they have been used in a series of stud-
198 ies to improve the monitorability and predictability of vadose zone processes using geo-
199 physical measurements (Binley & Beven, 2003; Binley, Cassiani, et al., 2002; Binley, Cas-
200 siani, & Winship, 2004; Binley, Winship, Middleton, Pokar, & West, 2001; Binley, Win-
201 ship, et al., 2002). Two radar and four ERT boreholes were drilled around an injector
202 to monitor tracer injection. Each ERT borehole consists of sixteen stainless steel mesh
203 electrodes equally spaced at 0.733 m between 2 and 13 m depth. The borehole electrodes
204 were supplemented with eight surface electrodes. Two cored boreholes were drilled close
205 to the tracer injection area to obtain a depth profile of grain size distribution. Note that
206 the top 2 meters is topsoil while its underlying material is weakly cemented sandstone.
207 A similar borehole ERT and GPR setup was applied for the monitoring experiment at
208 the Arreneas infiltration plant in Denmark (Haarder et al., 2012; Looms, Binley, Jensen,
209 Nielsen, & Hansen, 2008).

209 In this study, we fitted the Archie relationships for the cores collected at Eggbor-
210 ough and used them as realizations of petrophysical models. We then simulated the ERT
211 response of a water injection experiment, assuming a baseline petrophysical relationship.

We then inverted the ERT response and use each of the realizations of petrophysical models to estimate moisture content with uncertainty bounds, which we compared against the simulated value. We summarize the workflow of our approach in Figure 1.

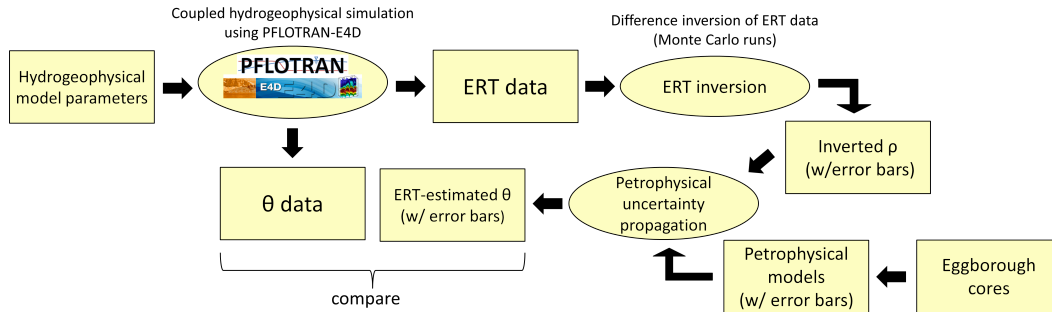


Figure 1. Moisture content (θ) estimation and petrophysical uncertainty propagation workflow used in this study. Rectangles indicate model inputs or data, while ovals represent modelling or analysis steps. We obtained synthetic ERT and θ data using PFLOTRAN-E4D. Then we inverted the ERT data and used the Eggborough cores as different petrophysical models. They were passed through the moisture content estimation and uncertainty estimation framework to obtain ERT-estimated θ , which were compared against the θ data.

2.1 Eggborough core samples

Core samples collected at Eggborough were used to measure the spectral induced polarization (SIP) responses at various saturations (Binley, Slater, Fukes, & Cassiani, 2005) and they are compared with various physical and hydraulic properties (Table S2). They found a strong correlation between mean relaxation time and hydraulic conductivity and showed that the former is affected by saturation. Binley et al. (2005) did not include the data showing the DC resistivity and hydraulic properties were not published. Also, they focused their analysis on only three of the samples extracted. In this work, we examine the DC resistivity-saturation behaviour of all the samples to understand its variability and the impact of such variability on estimating moisture content from ERT.

The grain size distribution of the Eggborough cores and blocks are plotted as percentiles (Figure 2a). Also, the percentages of sand, silt, clay at Eggborough are plotted as depth profiles (Figure 2b). Note that the cores are not repacked sample but instead they are weakly cemented core plugs. In this work, we use the Eggborough data to obtain petrophysical relationships for predicting moisture content in a water injection simulation.

2.2 Water injection simulation

The March 2003 tracer infiltration experiment at Hatfield (Binley, 2003; Winship, Binley, & Gomez, 2006) used a tracer that consisted of 1,200 litres (or 1.2 m^3) of water, dosed with NaCl to give an σ_f of $2,200 \mu\text{S cm}^{-1}$ (groundwater σ_f was $650 \mu\text{S cm}^{-1}$). The tracer was injected over a period of three days, from 14th March 2003 to 17th March 2003 at a steady rate of 17 L/h. The tracer injection port was screened between 3 m and 3.5 m below ground surface. The water table was at 10 m below ground surface. The layout of the electrodes is shown in Figure 5.

Since our focus here is the change in moisture content, we numerically repeat the Hatfield 2003 injection experiment with groundwater instead of a conductive tracer. We

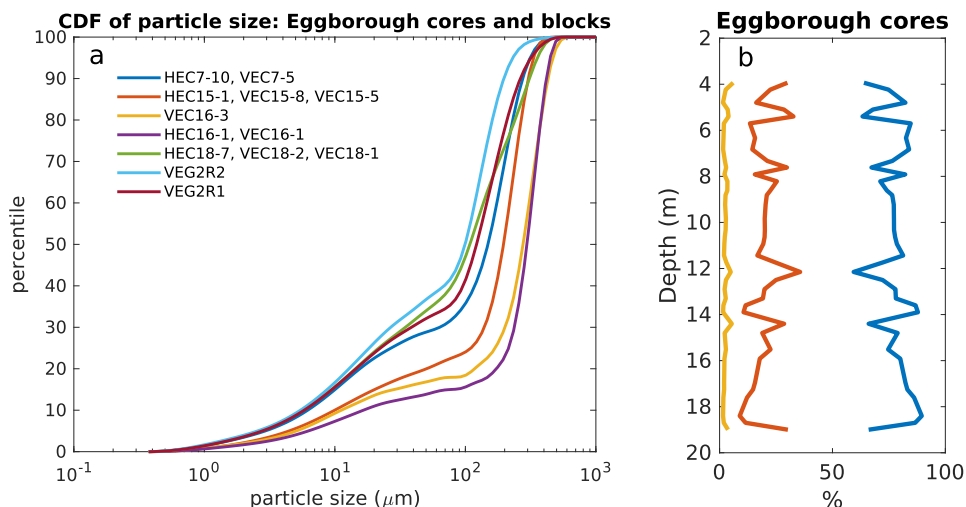


Figure 2. (a) Cumulative density functions of grain size distribution of Eggborough cores and blocks. The legend shows the core or block ID. (b) Depth profiles of sand, silt, and clay percentages for Eggborough cores.

used the parallel coupled hydrogeophysics code PFLOTRAN-E4D (Johnson, Hammond, & Chen, 2017) to simulate the flow and transport of the water injection and to obtain the corresponding ERT response. PFLOTRAN (Hammond, Lichtner, & Mills, 2014) is a subsurface flow and reactive transport code and we use the Richards model to simulate variably saturated flow. E4D (Johnson, Versteeg, Ward, Day-Lewis, & Revil, 2010) is a 3D modeling and inversion code designed for subsurface imaging and monitoring using static and time-lapse 3D electrical resistivity or spectral induced polarization data, which we use here as a forward ERT simulator. The PFLOTRAN grid consists of 129,600 cells that are 0.25m to 1m wide and 0.5m thick. The E4D mesh is an unstructured tetrahedral mesh generated by tetgen (Si, 2015). The resultant mesh comprises 8,124 nodes and 46,842 elements. PFLOTRAN-E4D interpolates and maps the PFLOTRAN outputs to electrical resistivity on the E4D mesh given element-wise petrophysical transform. ERT snapshots are taken on days 7, 9, 10, 15, 18, 21, 27, and 41. We assume a 2% measurement error in each of the 3,108 measurements taken in each frame. An additional 2.5% is added to the data errors in the inversions to account for forward modelling errors. The parameters used in the simulation can be found in Table 1. The assumed petrophysical parameters are also plotted in Figure 4.

2.3 Petrophysical models

2.3.1 Archie's Law

Assuming minimal contribution from electrical conductivity on the grain surface, Archie's Law relates bulk electrical resistivity ρ (1/conductivity) to fluid saturation S . It is given by:

$$\rho = \sigma_f^{-1} \phi^{-m} S^{-n} \quad (1)$$

where m is the cementation factor, σ_f is the fluid conductivity, ϕ is the porosity and n is the saturation exponent. Assuming constant material and fluid properties (e.g. m, n, σ_f), Archie's Law can be re-written in terms of the electrical resistivity at saturation (i.e. $S=1$), which is given by:

Table 1. Parameters used for the water injection experiment

Parameters	Value
Initial water saturation	0.375
Water fluid conductivity σ_f	650 $\mu S\ cm^{-1}$
Injector depth interval	3-3.5 m
Assumed Archie's n	1.35
Water injection rate	0.408 m^3/d
Assumed Archie's ρ_s (at 650 $\mu S/cm^{-1}$)	44 Ωm
Injection period	Days 8-11
Assumed ERT data errors	4.5%
Hydraulic conductivity	0.4 m/d
van Genuchten α	10 m^{-1}
Porosity	0.32
van Genuchten n	2.5

$$S = \left(\frac{\rho_s}{\rho} \right)^{\frac{1}{n}} \quad (2)$$

where $\rho_s = \sigma_f^{-1} \phi^{-m}$. To obtain best-fit estimates of Archie parameters, a straight line is fitted for $\log_{10}(S)$ and $\log_{10}(\rho_s)$ using the least-squares criterion. The fitting routine returns the covariance structure of the model estimates, which can be used to determine the 68% confidence interval (1 standard deviation) of the model estimates. Note that ρ_s corresponds to a particular σ_f . Therefore, it needs to be scaled when applied to a different σ_f using eq. (1). We note that constant fluid conductivity may not be appropriate in a range of environments (e.g. Altdorff et al., 2017). Because the clay content in the cores is low, the results from fitting the Waxman-Smiths model are not reported. Note that saturation and moisture content θ are related by $S = \theta/\phi$. The total amount of moisture V_w within a volume V is given by $\phi V S$.

The fractional change of θ , or equivalently that of S , is given by

$$\frac{\theta_t}{\theta_0} = \left(\frac{\rho_t \sigma_{f,t}}{\rho_0 \sigma_{f,0}} \right)^{-\frac{1}{n}} \quad (3)$$

where the subscripts t and 0 represent the variable at time t and at baseline.

2.4 ERT modeling and inversion

We use the code R3t version 1.8 (www.es.lancs.ac.uk/people/amb/Freeware/R3t/R3t.htm) for ERT inversion. To obtain the resistivity variation, we seek to find a model solution that minimizes the following objective function:

$$\Phi = \Phi_d + \Phi_m = (d - F(m))^T W_d^T W_d (d - F(m)) + \alpha m^T R m \quad (4)$$

where d is the data (e.g. measured apparent resistivities), $F(m)$ is the set of simulated data using the forward model and estimated parameters m . W_d is a data weight matrix, which, if we consider the case of uncorrelated measurement error and ignore forward model errors, is a diagonal matrix with entries equal to the reciprocal of the errors of each measurement. Forward modelling errors are also added to the diagonal of W_d . α is the scalar

regularisation factor, while R is a roughness matrix that describes the spatial connect-
 edness of the parameter cell values. α is selected via a line search and isotropic smooth-
 ing is applied.

Using a Gauss-Newton procedure, the above is solved iteratively using the follow-
 ing solution:

$$\begin{aligned} (J^T W_d^T W_d J + \alpha W_m^T W_m) \Delta m &= J^T W_d (d - F(m)) - \alpha R m_k \\ m_{k+1} &= m_k + \Delta m \end{aligned} \quad (5)$$

where J is the Jacobian (or sensitivity) matrix, given by $J_{i,j} = \partial d_i / \partial m_j$; m_k is the
 parameter set at iteration k ; and Δm is the parameter update at iteration k . For the
 DC resistivity case, the inverse problem is typically parameterized using log-transformed
 resistivities, which we have adopted here.

For analysis of time-lapse ERT, we follow the difference inversion approach (Labrecque
 and Yang, 2001) to invert on the change in ERT data. Its model penalty function seeks
 to minimize model variation relative to a reference model m_{ref} :

$$\Phi_m = \alpha (m - m_{ref})^T R (m - m_{ref}) \quad (6)$$

Again, using a Gauss-Newton procedure, the objective function can be solved it-
 eratively by:

$$\begin{aligned} (J^T W_d^T W_d J + \alpha R) \Delta m &= J^T W_d ((d - d_{ref}) - (F(m) - F(m_{ref}))) - \alpha R (m - m_{ref}) \\ m_{k+1} &= m_k + \Delta m \end{aligned} \quad (7)$$

where d_{ref} is the baseline data vector. This approach, which has been proven to
 be effective in removing the effect of systematic errors (e.g. artefacts), has been applied
 to numerous time-lapse imaging studies (Doetsch, Linde, Pessognelli, Green, & Gunther,
 2012; LaBrecque, Heath, Sharpe, & Versteeg, 2004). Note that the same mesh is used
 for both ERT forward modelling and inversion.

2.5 Uncertainty propagation and moisture content estimation

After inverting the electrical resistivity models, we can obtain the corresponding
 element-wise moisture content using the petrophysical relationships. The quantity of wa-
 ter within a certain volume is given by the spatial integral of the moisture content within
 the volume.

Rules of analytical uncertainty propagation (Chen & Fang, 1986; Taylor, 1982) were
 followed to propagate petrophysical uncertainty to moisture content estimates at each
 element. The uncertainty of saturation estimated from Archie's law is given by the fol-
 lowing equation (see Appendix 1 for details):

$$\sigma_S^2 = \left(\frac{\partial S}{\partial \rho} \right)^2 \sigma_\rho^2 + \left(\frac{\partial S}{\partial \rho_s} \right)^2 \sigma_{\rho_s}^2 + \left(\frac{\partial S}{\partial n} \right)^2 \sigma_n^2 \quad (8)$$

where σ^2 is the variance of parameters. $\sigma_{\rho_s}^2$ and σ_n^2 are determined by the param-
 eter fitting procedures. σ_ρ^2 are determined by running Monte Carlo simulations of ERT
 inversion (Aster, Borchers, & Thurber, 2005; Tso et al., 2017, see supplementary infor-
 mation for details). This procedure, in essence, samples the measurement errors based

on the prescribed error levels and obtains a distribution of inverted resistivity at each cell due to the perturbed measurements. The first term in the above equation can be viewed as the variance contribution from the variance of ERT inversion, while the other terms are the contributions from the uncertainty in the petrophysical fits. When evaluating the difference in saturation between two survey times, it is important to take account of the fact that their uncertainties may be correlated. Therefore, the variance of the difference in saturation ΔS is given by:

$$\sigma_{\Delta S} = \sqrt{\sigma_S^2 + \sigma_{S_0}^2 - 2 \text{cov}(S, S_0)} \quad (9)$$

where S_0 is saturation at baseline and $\text{cov}(S, S_0)$ is approximated by all the S values in the model domain at the two times. The variance of saturation can be converted to that of the total amount of water (V_w) within a volume by:

$$\sigma_{V_w}^2 = \left(\frac{\partial V_w}{\partial \phi}\right)^2 \sigma_\phi^2 + \left(\frac{\partial V_w}{\partial S}\right)^2 \sigma_S^2 = (VS)^2 \sigma_\phi^2 + (V\phi)^2 \sigma_S^2 \quad (10)$$

If porosity ρ is assumed to be known and constant, the first term is dropped. For a finite element domain consisting of many elements, the total variance is simply the sum of variances of all the elements.

3 Results

3.1 Fitting Archie models

Figure 3 shows the water saturation-electrical resistivity relationship of twelve of the Eggborough cores and blocks. Note that some sample exhibits rather large scatter and in a few occasions, the resistivity shows a decrease with decreasing saturation. Archie's Law is fitted on the data. The best-fit line and the corresponding ± 1 standard deviation envelope are also plotted. Both ρ_s (27.45 – 64.35 Ωm) and n (0.513-2.174) show significant variability. As observed in Table S1, the variability in Archie parameters does not tend to correlate with texture-related properties. In most previous studies literature-based estimates of Archie parameters are adopted and where laboratory analysis is carried out, only a few samples are used. The significant variability (within the same unit) and lack of correlation with other properties presented here illustrate the challenge of constraining Archie parameters in the field. Our data shows two distinct groups of clay contents ($\sim 2\%$ and $\sim 3.5\%$) and the corresponding Archie parameters show slightly different ranges. Figure 3 also shows the Archie's parameter estimation of all Eggborough cores and blocks. The predictions using the best-estimate of the parameters are shown in solid lines, while the 68% (i.e. ± 1 standard deviation) confidence intervals are shown in dashed lines. It shows that when fitting all of the cores and blocks together, the resultant standard deviation is low, leaving some data points outside the ± 1 standard deviation envelope. We have also included the fit for Hatfield cores reported in Binley, Winship, et al. (2002) and summarize all the Archie models in Figure 4. Further details, including hydraulic and surface area measurements, of the Eggborough cores and blocks can be found in Table S2.

3.2 Moisture content estimation for the water injection simulation

The time-lapse ERT monitoring data during the water injection simulation was inverted using a difference inversion as described above. The iso-surfaces in Figure S1 show a volume that has 5.5% reduction of resistivity relative to baseline (Day 7). The inversion results capture the geometry and the swell-shrink dynamics of the plume very well. The plume expanded gradually once the injection commenced and then migrated downwards within a few days after the injection finished.

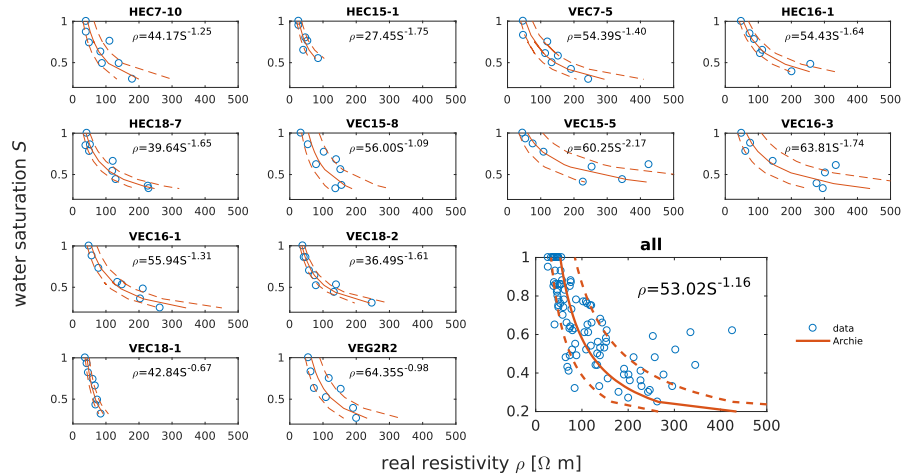


Figure 3. Archie's parameter estimation of individual Eggborough cores and blocks. The predictions using the best estimate of the parameters are shown in solid lines, while the 68% (i.e. ± 1 standard deviation) confidence intervals are shown in dashed lines. Note that the measurements are made at $1000 \mu\text{S cm}^{-1}$. Note that ρ , which is the dependent variable, is shown on the x-axis.

Our subsequent results focus on an ERT snapshot 10 days after the injection (Day 18). Figure 5a-b show the resultant mean and standard deviation of electrical resistivities obtained from Monte Carlo runs of ERT inversion. Since we have assumed uniform initial saturation, the variation of resistivity is within the same order of magnitude. The centre region of the ERT array shows reduced resistivity due to injection. The standard deviation is higher around the electrodes and is lower in the centre region because the resolution of ERT decreases away from electrodes. Conceptually, however, the uncertainty in the centre region through which the water plume evolves should be higher. This issue is not addressed in this study. Based on the Monte Carlo inversion results, Figure 5c shows the volume extracted from the ERT inversion domain where there is at least a 5.5% reduction in resistivity on Day 18 relative to the pre-injection baseline (Day 7). Such a threshold is used so that the effects of inversion artefacts are minimized. The size of this volume is 79.97 m^3 . The total amount of water in this volume at Day 7 and Day 18 are 9.65 m^3 and 10.68 m^3 respectively. The resistivities on the nodes of the extracted volume were converted to saturation using the different petrophysical relationships (i.e. Archie model fits) discussed above, while a Monte Carlo experiment was run to estimate the uncertainty in the inverted resistivities.

For each of the petrophysical models, we then integrate the moisture contents over the extracted volume to estimate the total water volume (V_w) in it. At the same time, we derive error bars for the total water volume estimates using eq. 8 and 9. Figure 6a shows the mean and uncertainty bounds for the amount of water within the extracted volume, assuming a constant porosity of 0.32. For Day 18 (post-injection), best-estimates of total water volume among Archie models lies between 8.70 m^3 (Binley02) to 16.74 m^3 (VEC15-5), except for VEG2R1 and VEC18-1 it lies at 2.51 and 3.88 m^3 , respectively. The size of the error bars varies between $\pm 0.68 \text{ m}^3$ (VEG2R1) and $\pm 2.28 \text{ m}^3$ (VEC15-8), or between 9.59% (VEC18-2) and 27.01% (VEG2R1), depending on the Archie parameters estimates and their uncertainties. We observe similar results for Day 7 (pre-injection); yet we note that while the size of the error bars generally increases from Day 7 to Day 18, the increase ranges from 0.19 m^3 (HEC15-1) to 0.72 m^3 ("all").

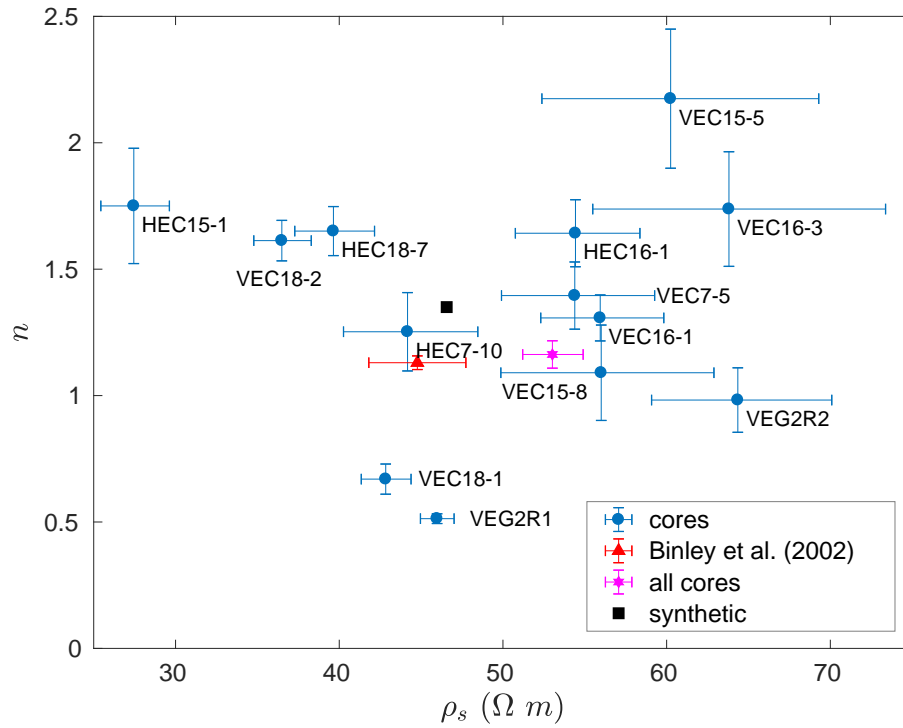


Figure 4. Summary of Archie model fits for the Eggborough/Hatfield cores and blocks. Note that values correspond to $\sigma_f = 1000\mu S\ cm^{-1}$. The point label "synthetic" is the "true" solution considered in the synthetic study in section 3.2.

Figure 6b shows the *change* in total water volume on Day 18 relative to baseline. The mean *change* is the difference between the total water volume at the two times. Using eq. 10, the error bars shown here have accounted for potential correlation between total water volume estimates between the two times. As a result, when fluid conductivity is assumed constant, the uncertainty bounds for the change in total moisture would lie between one and two times of that of the total moisture. The Archie models estimate an increase in mean *change* in total water volume of $0.46\ m^3$ (VEG2R1) – $1.08\ m^3$ (VEG2R2). They are more consistent than the estimates of the absolute total water volume. Note that, the total injection volume was $1.224\ m^3$, meaning all the models have underestimated the addition of water due to injection. The uncertainty bounds in Figure 6b are generally large, ranging from $\pm 0.71\ m^3$ (VEG2R1) to $\pm 2.96\ m^3$ (VEC15-8), or 154% (VEG2R1) to 350% (HEC15-1) of the mean value. This shows that even though the mean estimates for the *change* in total water volume using Archie models is consistent, they are nevertheless highly uncertain.

The size of the error bars in Figure 6a is determined by a combination of the uncertainty of the petrophysical parameters (ρ_s and n) and that of the inverted resistivities ρ . Based on eq. 8 and 9, the variance of the total moisture estimates is the summation of the squared product of the partial derivative and standard deviation of the individual terms. We plot the terms as stacked bars for Day 18 (post-injection) in Figure 6c to show their contribution to the total variance. The square root of the total height of the bars equals the size of the error bars in Figure 6a. The contribution from inverted resistivities ρ is below $2\ (m^3)^2$ for all the Archie models. For the Archie models with variance smaller than $2\ (m^3)^2$, inverted resistivities can be an important source of errors;

otherwise, the effects of uncertain petrophysical parameters dominate. Our results indicate that for the Archie models, n plays a more important role than ρ_s , with the exception of Binley02, which shows very low n error. n contributes 3.88% (VEG2R1) to 69.25% (HEC15-1) of the total variance, while ρ_s contributes 2.55% (VEG2R1) to 36.71% (VEC16-3) of the total variance.

So far we have assumed the porosity has a constant value of 0.32. Additional uncertainty is introduced if it is treated as uncertain. We consider the case where porosity is assumed to be 0.32 ± 0.032 . In Figure 6d, the height of the blue bars is the total height of the bars in Figure 6c. The height of the yellow bars shows the additional variance due to the uncertain porosity value, which ranges from $0.0631 \text{ (m}^3\text{)}^2$ (VEG2R1) to $2.8026 \text{ (m}^3\text{)}^2$ (VEC15-5). Percentage-wise, the uncertain porosity values lead to an increase in variance ranging from 13.7% (VEG2R1) to 108% (VEC18-2).

We have examined in Figure 6b the change in total moisture within the extracted volume. We examine in Figure 7 the change in volume of water within each finite element cell of the extracted volume. Figure 7a shows the estimated change in the volume of water (V_w) in four selected cells. It is observed that while the true change spans from 0 to 0.18 m^3 , the estimates for Archie models stays within the 0 to 0.05 m^3 range. Figure 7b shows the scatter plots for the ERT-estimated V_w using the 15 Archie models. For all of them, the fit at individual cells is unsatisfactory. Conversely, in Figure 6b the changes in total moisture within the extracted volume are fairly consistent across the petrophysical models and they agree with the true value. We observe that within the extracted volume (the threshold was change in inverted resistivity greater than 5.5%), 101 of 219 cells show change in saturation of less than 0.01. This indicates the true water plume is much narrower than estimated by ERT inversion and highlights the detection limit of ERT, particularly in the context of smoothness-constrained inversion used here. The smoothing effect of the ERT inversion, however, roughly preserves mass balance in this case.

4 Discussion and implications for future work

4.1 Fitting petrophysical models

Most previous studies have either fitted petrophysical models for up to a few cores or used petrophysical parameters based on literature values without assuming any errors or uncertainty. Our results from cores collected at a relatively uniform and clay-free sandstone unit suggest that in future studies, a wider range of petrophysical relationships or a larger uncertainty bound should be assumed. The n and ρ_s estimates do not appear to show significant correlation with other properties that were measured, making it difficult to constrain petrophysical relationships with more core samples. In fact, compared with previous studies at Hatfield and Eggborough, the use of more core data reveals greater petrophysical model uncertainty. The individual Archie model fits are good but the concatenated dataset shows a U-shape $\theta(\rho)$ behaviour, which suggests saturation is controlled by properties other than a saturation exponent or it implies a heterogeneous petrophysical parameter field.

4.2 The uncertainty propagation approach

We have proposed and demonstrated an effective procedure to propagate uncertainties in petrophysical relationships to uncertainties in the inferred moisture contents and the amount of water within the plume. The procedure requires mean and standard deviation of both the petrophysical parameters and inverted resistivities. The application of this method on field data using two types of petrophysical models shows how uncertainty in petrophysical parameters and ERT data errors propagate through the modelling and inversion process and lead to uncertainty in moisture content estimates. Specif-

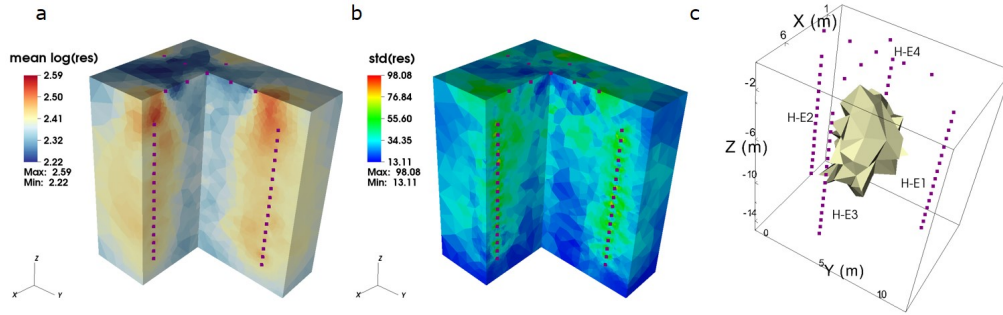


Figure 5. (a) Mean (\log_{10}) and (b) standard deviation (linear) of electrical resistivity for Day 18 obtained from Monte Carlo runs of ERT inversion. (c) Extracted volume where there was a 5.5% reduction of resistivity relative to baseline on Day 18. The purple cubes are electrode locations.

ically, the inversion procedure smooths the resistivity profiles (a proxy of moisture content) spatially, while the uncertain petrophysical relationships add uncertainties to the quantitative conversion from resistivity to moisture content. These uncertainties, if untracked, can lead to significant bias and over-confidence in the moisture content estimates.

Part of our analysis has utilized a commonly employed smoothness-based inversion for our geophysical data to evaluate the impact of uncertain petrophysical relationship. Other inversion algorithms may yield different uncertainty estimates. In fact, a limitation of this work is that our computation of the uncertainty contribution from inverted resistivity only considered the propagation of data errors through the inversion code. We have assumed no uncertainty contribution from the choice of the inverse model, its resolution, or its discretization, mainly because there is no standard procedure to compute the uncertainty of an inverted resistivity field yet. Some emerging techniques, such as trans-dimensional ERT (Galetti & Curtis, 2018), are attempts to address this issue. We also acknowledge Markov chain Monte Carlo (MCMC) sampling (Brunetti & Linde, 2018) may be more accurate and robust than the conventional MC sampling we use here.

Finally, we note that our approach follows the classical approach to error analysis (Taylor, 1982). The extent to which some of the underlying assumptions are valid, such as whether the uncertainties of petrophysical parameters and inverted resistivities are independent, is open to future investigation. Nevertheless, we highlight that the uncertainty propagation framework presented in this work is flexible and straightforward. It is potentially applicable to any type of petrophysical models and inversion methods and it may be extended to consider the uncertainty of the inversion itself. It is independent of the inversion methods and petrophysical models used, and we expect it to be used widely in future studies.

4.3 Total moisture content estimation

The great variety of petrophysical models lead to a large range of total water volume estimates (Figure 6a). This shows that using only a single petrophysical model deterministically can give misleading results. It also shows that any applications wishing to quantify the absolute amount of moisture present must not rely on geophysics alone. The changes in moisture content estimated by Archie's law, however, are generally consistent (Figure 6b). This can be explained by the work of Lehmann et al. (2013), who show that the fractional changes in moisture content obtained from electrical resistivity are a scaling of the saturation exponent only. This means the other parameters in

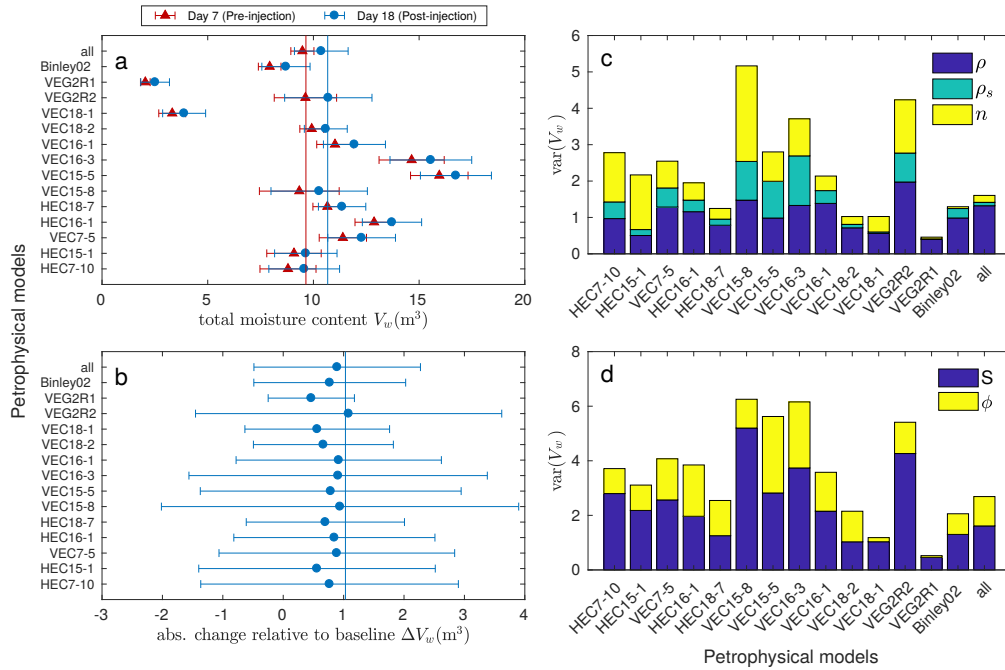


Figure 6. (a) Total water volume within the extracted volume (with uncertainty bounds) using the different petrophysical models. The uncertainty bounds correspond to ± 1 standard deviation. The vertical lines show the true total water volume. (b) The corresponding changes in the amount of moisture within the extracted volume relative to baseline. The vertical lines show the true change in total water volume. (c) The contribution of different variables to the variance of total moisture of each petrophysical models. (d) Additional variance (i.e. uncertainty) caused by uncertain porosity values (0.32 ± 0.032). The contribution from uncertain porosity is significant in most cases, especially when the variance in saturation is low.

simple empirical models do not play a role in converting ratios of inverted resistivities to ratios of θ . Nevertheless, most applications are interested in at least the difference of moisture content between two times, not just their relative change. We note the high uncertainty bounds associated with the change in θ obtained from most of the Archie petrophysical models. This shows that this scaling of n can lead to highly uncertain estimates of the amount of the change. This effect should be acknowledged and assumed when interpreting ERT-derived moisture contents. Moreover, other parameters in petrophysical models are still important in other frequently used methods. For example, coupled modelling of hydrogeophysics requires reliable petrophysical relationships. Examining the impact of the different uncertain petrophysical parameters and models remains an important research question.

Our uncertainty analysis shows that for most cases, the uncertainty in ERT-derived saturation is dominated by uncertain petrophysical parameters, not uncertain inverted resistivities due to data errors (Figure 6c). This presents a challenge because unlike inverted resistivities, petrophysical uncertainties cannot be straightforwardly reduced by good quality data or better inverse modelling approaches. Future studies should focus their efforts on better characterizing petrophysical uncertainties and incorporating them in moisture content estimation procedures. Figure 6d also shows that significant additional uncertainty can be caused by uncertain porosity values. Since porosity ultimately

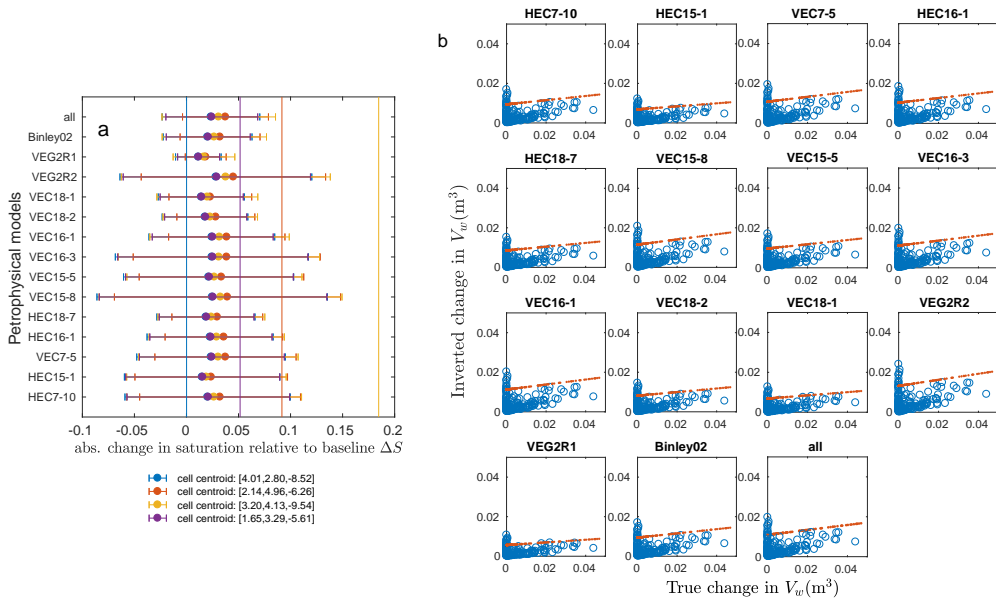


Figure 7. (a) ERT estimated changes in volume of water in 4 selected cells. The vertical lines indicate the true change. (b) Scatter plots showing the fit for change in volume of water at individual cells using the 15 Archie models. The red dashed line in each plot is the best-fit line of the scatter points.

controls the volume of pore space for water to fill, better characterization of it can reduce the uncertainty of the moisture content estimates from ERT.

Our work has focused on a water injection experiment where there is no variation in fluid conductivity over time. Changes in fluid conductivity (e.g. in a saline tracer injection or leak of saline solute) will further complicate the estimation of moisture content changes since bulk resistivity is affected by both fluid conductivity and moisture content. When inverting time-lapse ERT data, the change relative to baseline is often set to be minimized. This setting works well in our water injection experiment but may give an insufficient change in resistivity to account for both changes in saturation and fluid conductivity.

Since laboratory petrophysical measurements are labour-intensive and time-consuming, many authors have used TDR data (in shallow vadose zone investigations) to fit field-based petrophysical relationships (e.g. Fan, Scheuermann, Guyot, Baumgartl, & Lockington, 2015). The typical setup, for shallow investigations, consists of a trench with ERT, TDR, and temperature sensors installed. This *in-situ* setup can be viewed as advantageous over lab measurements since it correctly represents pore water conductivity (given dynamic exchange of ions between particles and pore water) and avoids forced conditions in the lab. Despite its advantages, the range of ρ it considers is limited because only the range of the ERT-measured apparent ρ are evaluated. Given the large variability of petrophysical relationships observed in this study, perhaps the TDR data is best used to independently verify or constrain the inverted moisture contents (e.g. Beff et al., 2013). It is important to check independently whether the uncertainty bounds of ERT-predicted moisture content consistently capture the TDR data. While TDR or neutron probe can only be applied in shallow soil, radar can be used in deeper investigations. The joint use of ERT and radar measurements (e.g. Binley, Cassiani, et al., 2002; Linde et al., 2006) yields independent estimates of moisture contents and allows cross-validation.

We have examined the changes in total moisture content in the extracted volume and at selected locations obtained from ERT and their agreement with the simulation. Future uncertainty studies should consider the agreement by comparing ERT estimates and other (e.g. TDR, neutron probe) data in the field. Further work should also examine the extent to which the uncertainty in ERT-derived moisture content affects the decision-making in specific applications, such as landslide monitoring or precision agriculture.

4.4 Strategy when petrophysical data is unavailable

With the increasing popularity of ERT or EMI studies for hydrological investigations, there will be an increasing number of studies that do not collect samples for petrophysical calibration, which is often more time-consuming than the geophysical survey itself. Conversely, a few depth profiles of grain size distributions are relatively easy to obtain (e.g. using a hand auger) in near-surface applications. Soil texture is commonly used to approximate unsaturated zone parameters through pedotransfer functions (e.g. ROSETTA (Schaap, Leij, & van Genuchten, 2001; Zhang, Schaap, Guadagnini, & Neuman, 2016)) and it will be useful if these functions can approximate the petrophysical parameters or models too. Future efforts should be devoted to building a global database on $\theta(\rho)$ and grain size distribution data, in order to formulate pedotransfer functions across sites. Data-driven methods such as multiple adaptive regression splines (MARS) (Brihlante et al., 2014) are particularly suitable for this task because they are capable of handling fairly large datasets (e.g. 105 observations and 100 variables). We attempted to apply some of these methods to fit the Eggborough data (not reported here) but we have too few samples to apply them reliably. Nevertheless, they are potentially powerful methods to apply in the future once there is a database for near-surface petrophysical measurements.

4.5 Relevance to EMI and other geophysical methods

We have focused mainly on the effect on ERT inversion results, but similar conclusions can be extended for EMI results or methods that use a combination of EMI and ERT results (von Hebel et al., 2014), as well as other applications in hydrogeophysics where petrophysical transforms are involved. Moreover, we recognize that there is a wealth of literature studying the spatial and temporal patterns of electrical conductivity and soil moisture in the Earth's near-surface. Similarly, there have been many recent studies on data assimilation of moisture content data across multiple spatial scales (e.g. Zhu et al., 2017). Hydrogeophysicists, whilst frequently working at the plot-scale and site-scale, should be involved in these developments. Closer collaboration between soil scientists, geostatisticians, geophysicists, and hydrologists are needed to tackle this grand challenge.

5 Conclusions

Our study showed the extent of petrophysical variability present at a field site and demonstrated an approach to computing uncertainty bounds of moisture content estimates due to uncertain petrophysical models. First, we showed that highly variable petrophysical relationships can be observed in field samples of a relatively uniform and clay-free sandstone unit. We then fitted and applied various petrophysical models to convert ERT images to moisture content images. The different petrophysical models led to a wide range of total moisture content estimates of a plume, but their *changes* over time generally agreed. Using rules of error propagation, we were able to quantify the uncertainty bounds of the moisture content estimates and gained further insight by showing the individual contribution of the petrophysical parameters and inverted resistivities terms to the total uncertainty. We showed that, assuming the inverse model only smooths the resistivity field, the uncertainty is dominated by the petrophysical parameters. The total

uncertainty was found to be 7.52% - 23.18% of the mean total water volume estimate. When translated to the *change* in time, the uncertainty can be as high as several multiples of the mean estimate—both uncertainties are higher than previously appreciated.

Our results have highlighted the potential danger of converting ERT images to moisture content from similar environments using a single petrophysical model deterministically. In particular, they should not be used to quantify the amount of moisture present independently of other data. Although the different Archie petrophysical models give consistent estimates of the change in total water volume, their relatively large uncertainty bounds highlight that even though electrical geophysics reliably determines the direction of the change in θ , its quantification of the amount of such change is highly uncertain. It is prudent to assume large uncertainties for θ and $\Delta\theta$ estimates where they have not been quantified. Data-driven methods (e.g. MARS) have the potential to be applied to build petrophysical models where such data is unavailable.

Appendix: Petrophysical uncertainty propagation

Following the analytical sensitivity analysis of Chen and Fang (1986) and Taylor (1982), we can obtain the uncertainty contributions of the various terms in Archie's Law (eq. 2). Assuming they have uncorrelated errors, by laws of error propagation, the variance of saturation is given by:

$$\sigma_S^2 = \left(\frac{\partial S}{\partial \rho_s}\right)^2 \sigma_{\rho_s}^2 + \left(\frac{\partial S}{\partial \rho}\right)^2 \sigma_{\rho}^2 + \left(\frac{\partial S}{\partial n}\right)^2 \sigma_n^2$$

where

$$\begin{aligned}\frac{\partial S}{\partial \rho_s} &= \frac{1}{n\rho_s} S \\ \frac{\partial S}{\partial \rho} &= \frac{1}{n\rho} S \\ \frac{\partial S}{\partial n} &= \frac{\ln(\rho/\rho_s)}{n^2} S\end{aligned}$$

So

$$\begin{aligned}\left(\frac{\partial S}{\partial \rho_s}\right)^2 \sigma_{\rho_s}^2 &= \left(\frac{S}{n}\right)^2 \left(\frac{\sigma_{\rho_s}}{\rho_s}\right)^2 \\ \left(\frac{\partial S}{\partial \rho}\right)^2 \sigma_{\rho}^2 &= \left(\frac{S}{n}\right)^2 \left(\frac{\sigma_{\rho}}{\rho}\right)^2 \\ \left(\frac{\partial S}{\partial n}\right)^2 \sigma_n^2 &= \left(\frac{S}{n}\right)^2 \left(\frac{\ln(\rho/\rho_s)}{n} \sigma_n\right)^2\end{aligned}$$

Acknowledgments

This paper is published with the permission of the Executive Director of the British Geological Survey (NERC) and UK Nuclear Decommissioning Authority (NDA). The first author is supported by a Lancaster University Faculty of Science and Technology PhD studentship and an NDA PhD Bursary. Peter Winship (deceased) and Melanie Fukes conducted the field experiments and the laboratory analysis, respectively. We thank Jared West (Leeds University) for supplying the Hatfield core analysis. We thank Tim Johnson (Pacific Northwest National Laboratory) for assistance in using PFLOTRAN-E4D, access to the PNNL computing facilities, and hosting the first author's visits. We thank Keith Beven for commenting on an initial version of the manuscript. We are grateful to associate editor Sander Huisman, Sarah Garré, and an anonymous reviewer for their constructive comments. The data used in this paper is deposited at the Lancaster University's research data repository and is available for download through the following link:

<https://dx.doi.org/10.17635/lancaster/researchdata/293>

References

- Ahmed, M. A., Passioura, J., & Carminati, A. (2018). Hydraulic processes in roots and the rhizosphere pertinent to increasing yield of water-limited grain crops: A critical review. *Journal of Experimental Botany*, *69*(13), 3255–3265. doi: 10.1093/jxb/ery183
- Altdorff, D., von Hebel, C., Borchard, N., van der Kruk, J., Bogena, H. R., Vereecken, H., & Huisman, J. A. (2017). Potential of catchment-wide soil water content prediction using electromagnetic induction in a forest ecosystem. *Environmental Earth Sciences*, *76*(3), 111. doi: 10.1007/s12665-016-6361-3
- Amidu, S. A., & Dunbar, J. A. (2007). Geoelectric Studies of Seasonal Wetting and Drying of a Texas Vertisol. *Vadose Zone Journal*, *6*(3), 511. doi: 10.2136/vzj2007.0005
- Aster, R., Borchers, B., & Thurber, C. H. (2005). *Parameter estimation and inverse problems*. Burlington, Massachusetts, USA: Elsevier.
- Bass, B., Cardenas, M. B., & Befus, K. M. (2017). Seasonal shifts in soil moisture throughout a semiarid hillslope ecotone during drought: A geoelectrical view. *Vadose Zone Journal*, *0*(0), 0. doi: 10.2136/vzj2016.11.0108
- Beff, L., Günther, T., Vandoorne, B., Couvreur, V., & Javaux, M. (2013). Three-dimensional monitoring of soil water content in a maize field using electrical resistivity tomography. *Hydrology and Earth System Sciences*, *17*(2), 595–609. doi: 10.5194/hess-17-595-2013
- Binley, A. (2003). *Vadose Zone Tracer Testing in the UK Sherwood Sandstone : Hydrogeophysical Data Report* (Tech. Rep.). Livermore, California: Lawrence Livermore National Laboratory.
- Binley, A., & Beven, K. (2003). Vadose zone flow model uncertainty as conditioned on geophysical data. *Groundwater*, *41*(2), 119–127.
- Binley, A., Cassiani, G., Middleton, R., & Winship, P. (2002). Vadose zone flow model parameterisation using cross-borehole radar and resistivity imaging. *Journal of Hydrology*, *267*(3-4), 147–159. doi: 10.1016/S0022-1694(02)00146-4
- Binley, A., Cassiani, G., & Winship, P. (2004). Characterization of heterogeneity in unsaturated sandstone using borehole logs and cross-borehole tomography, in: *Aquifer Characterization*. In *Aquifer characterization* (pp. 129–138). SEPM (Society for Sedimentary Geology). doi: 10.2110/pec.04.80.0129
- Binley, A., Hubbard, S. S., Huisman, J. A., Revil, A., Robinson, D. A., Singha, K., & Slater, L. D. (2015). The emergence of hydrogeophysics for improved understanding of subsurface processes over multiple scales. *Water Resources Research*, *51*, 3837–3866. doi: 10.1002/2015WR017016
- Binley, A., Slater, L. D., Fukes, M., & Cassiani, G. (2005). Relationship between spectral induced polarization and hydraulic properties of saturated and unsaturated sandstone. *Water Resources Research*, *41*, W12417. doi: 10.1029/2005WR004202
- Binley, A., Winship, P., Middleton, R., Pokar, M., & West, J. (2001). High-resolution characterization of vadose zone dynamics using cross-borehole radar. *Water Resources Research*, *37*(11), 2639–2652. doi: 10.1029/2000WR000089
- Binley, A., Winship, P., West, L., Pokar, M., & Middleton, R. (2002). Seasonal variation of moisture content in unsaturated sandstone inferred from borehole radar and resistivity profiles. *Journal of Hydrology*, *267*(3-4), 160–172. doi: 10.1016/S0022-1694(02)00147-6
- Bouchedda, A., Chouteau, M., Binley, A., & Giroux, B. (2012, mar). 2-D joint structural inversion of cross-hole electrical resistance and ground penetrating radar data. *Journal of Applied Geophysics*, *78*, 52–67. doi:

- 10.1016/j.jappgeo.2011.10.009
- 675 Brillante, L., Bois, B., Mathieu, O., Bichet, V., Michot, D., & Lévêque, J. (2014).
676 Monitoring soil volume wetness in heterogeneous soils by electrical resistivity.
677 A field-based pedotransfer function. *Journal of Hydrology*, *516*, 56–66. doi:
678 10.1016/j.jhydrol.2014.01.052
- 679 Brillante, L., Mathieu, O., Bois, B., Van Leeuwen, C., & Lévêque, J. (2015). The
680 use of soil electrical resistivity to monitor plant and soil water relationships in
681 vineyards. *Soil*, *1*(1), 273–286. doi: 10.5194/soil-1-273-2015
- 682 Brunet, P., Clément, R., & Bouvier, C. (2010). Monitoring soil water content
683 and deficit using electrical resistivity tomography (ERT) - a case study in
684 the Cevennes area, France. *Journal of Hydrology*, *380*(1-2), 146–153. doi:
685 10.1016/j.jhydrol.2009.10.032
- 686 Brunetti, C., & Linde, N. (2018). Impact of petrophysical uncertainty on Bayesian
687 hydrogeophysical inversion and model selection. *Advances in Water Resources*,
688 *111*(July 2017), 346–359. doi: 10.1016/j.advwatres.2017.11.028
- 689 Brunetti, C., Linde, N., & Vrugt, J. A. (2017). Bayesian model selection in hydro-
690 geophysics: Application to conceptual subsurface models of the South Oyster
691 Bacterial Transport Site, Virginia, USA. *Advances in Water Resources*, *102*,
692 127–141. doi: 10.1016/j.advwatres.2017.02.006
- 693 Cassiani, G., & Binley, A. (2005). Modeling unsaturated flow in a layered for-
694 mation under quasi-steady state conditions using geophysical data con-
695 straints. *Advances in Water Resources*, *28*(5), 467–477. doi: 10.1016/
696 j.advwatres.2004.12.007
- 697 Cassiani, G., Godio, A., Stocco, S., Villa, A., Deiana, R., Frattini, P., & Rossi, M.
698 (2009). Monitoring the hydrologic behaviour of a mountain slope via time-
699 lapse electrical resistivity tomography. *Near Surface Geophysics*, *7*(5-6),
700 475–486. doi: 10.3997/1873-0604.2009013
- 701 Chambers, J., Gunn, D., Wilkinson, P., Meldrum, P., Haslam, E., Holyoake, S.,
702 ... Wragg, J. (2014). 4D electrical resistivity tomography monitoring of
703 soil moisture dynamics in an operational railway embankment. *Near Surface*
704 *Geophysics*, *12*(1), 61–72. doi: 10.3997/1873-0604.2013002
- 705 Chen, H., & Fang, J. (1986). Sensitivity analysis of the parameters in Archie's wa-
706 ter saturation equation. *The Log Analyst*, *27*(5), 39–44. doi: SPWLA-1986
707 -vXXVIIIn5a3
- 708 Doetsch, J., Linde, N., Pessognelli, M., Green, A. G., & Gunther, T. (2012). Con-
709 straining 3-D electrical resistance tomography with GPR reflection data for
710 improved aquifer characterization. *Journal of Applied Geophysics*, *78*, 68–76.
711 doi: 10.1016/j.jappgeo.2011.04.008
- 712 Fan, J., Scheuermann, A., Guyot, A., Baumgartl, T., & Lockington, D. A. (2015).
713 Quantifying spatiotemporal dynamics of root-zone soil water in a mixed forest
714 on subtropical coastal sand dune using surface ERT and spatial TDR. *Journal*
715 *of Hydrology*, *523*, 475–488. doi: 10.1016/j.jhydrol.2015.01.064
- 716 Friedman, S. P. (2005). Soil properties influencing apparent electrical conductivity:
717 A review. *Computers and Electronics in Agriculture*, *46*(1-3), 45–70. doi: 10
718 .1016/j.compag.2004.11.001
- 719 Galetti, E., & Curtis, A. (2018). Transdimensional electrical resistivity tomography.
720 *Journal of Geophysical Research: Solid Earth*. doi: 10.1029/2017JB015418
- 721 Garré, S., Coteur, I., Wonglecharoen, C., Kongkaew, T., Diels, J., & Vanderborght,
722 J. (2013). Noninvasive monitoring of soil water dynamics in mixed crop-
723 ping systems: A case study in Ratchaburi Province, Thailand. *Vadose Zone*
724 *Journal*, *12*(2), 0. doi: 10.2136/vzj2012.0129
- 725 Garré, S., Javaux, M., Vanderborght, J., Pagès, L., & Vereecken, H. (2011). Three-
726 dimensional electrical resistivity tomography to monitor root zone water dy-
727 namics. *Vadose Zone Journal*, *10*(1), 412. doi: 10.2136/vzj2010.0079
- 728 Glover, P. W. (2015). Geophysical Properties of the Near Surface Earth: Electrical
729

- 730 Properties. In *Treatise on geophysics* (Vol. 11, pp. 89–137). Elsevier. doi: 10
731 .1016/B978-0-444-53802-4.00189-5
- 732 Glover, P. W. (2017). A new theoretical interpretation of Archie’s saturation expo-
733 nent. *Solid Earth*, 8(4), 805–816. doi: 10.5194/se-8-805-2017
- 734 Green, C. T., Liao, L., Nolan, B. T., Juckem, P. F., Shope, C. L., Tesoriero, A. J., &
735 Jurgens, B. C. (2018). Regional variability of nitrate fluxes in the unsaturated
736 zone and groundwater, Wisconsin, USA. *Water Resources Research*, 54(1),
737 301–322. doi: 10.1002/2017WR022012
- 738 Haarder, E. B., Binley, A., Looms, M. C., Doetsch, J., Nielsen, L., & Jensen, K. H.
739 (2012). Comparing plume characteristics inferred from cross-borehole geophys-
740 ical data. *Vadose Zone Journal*, 11(4), 1–40. doi: 10.2136/vzj2012.0031
- 741 Hammond, G. E., Lichtner, P. C., & Mills, R. T. (2014). Evaluating the per-
742 formance of parallel subsurface simulators: An illustrative example with
743 PFLOTRAN. *Water Resources Research*, 50(1), 208–228. doi: 10.1002/
744 2012WR013483
- 745 Hen-Jones, R. M., Hughes, P. N., Stirling, R. A., Glendinning, S., Chambers,
746 J. E., Gunn, D. A., & Cui, Y. J. (2017). Seasonal effects on geophysical-
747 geotechnical relationships and their implications for electrical resistivity to-
748 mography monitoring of slopes. *Acta Geotechnica*, 12(5), 1159–1173. doi:
749 10.1007/s11440-017-0523-7
- 750 Hermans, T., Nguyen, F., & Caers, J. (2015). Uncertainty in training image-
751 based inversion of hydraulic head data constrained to ERT data: Workflow
752 and case study. *Water Resources Research*, 51, 5332–5352. doi: 10.1002/
753 2014WR016259
- 754 Hinnell, A. C., Ferr, T. P. A., Vrugt, J. A., Huisman, J. A., Moysey, S., Rings, J., &
755 Kowalsky, M. B. (2010). Improved extraction of hydrologic information from
756 geophysical data through coupled hydrogeophysical inversion. *Water Resources*
757 *Research*, 46(4), 1–14. doi: 10.1029/2008WR007060
- 758 Hübner, R., Heller, K., Günther, T., & Kleber, A. (2015). Monitoring hillslope
759 moisture dynamics with surface ERT for enhancing spatial significance of hy-
760 drometric point measurements. *Hydrology and Earth System Sciences*, 19(1),
761 225–240. doi: 10.5194/hess-19-225-2015
- 762 Jayawickreme, D. H., van Dam, R. L., & Hyndman, D. W. (2008). Subsurface imag-
763 ing of vegetation, climate, and root-zone moisture interactions. *Geophysical*
764 *Research Letters*, 35(18), 1–5. doi: 10.1029/2008GL034690
- 765 Johnson, T. C., Hammond, G. E., & Chen, X. (2017). PFLOTRAN-E4D: A
766 parallel open source PFLOTRAN module for simulating time-lapse elec-
767 trical resistivity data. *Computers and Geosciences*, 99, 72–80. doi:
768 10.1016/j.cageo.2016.09.006
- 769 Johnson, T. C., Versteeg, R. J., Ward, A., Day-Lewis, F. D., & Revil, A. (2010).
770 Improved hydrogeophysical characterization and monitoring through parallel
771 modeling and inversion of time-domain resistivity and induced-polarization
772 data. *Geophysics*, 75(4), WA27. doi: 10.1190/1.3475513
- 773 Jonard, F., Bogena, H., Caterina, D., Garré, S., Klotzsche, A., Monerris, A., . . . von
774 Hebel, C. (2018). Ground-based soil moisture determination. In X. Li &
775 H. Vereecken (Eds.), *Observation and measurement of ecohydrological processes*
776 (pp. 1–42). Springer. doi: 10.1007/978-3-662-47871-4_2-1
- 777 Koestel, J., Kemna, A., Javaux, M., Binley, A., & Vereecken, H. (2008). Quan-
778 titative imaging of solute transport in an unsaturated and undisturbed soil
779 monolith with 3-D ERT and TDR. *Water Resources Research*, 44(12), 1–17.
780 doi: 10.1029/2007WR006755
- 781 Kuhl, A. S., Kendall, A. D., Van Dam, R. L., & Hyndman, D. W. (2018). Quanti-
782 fying soil water and root dynamics using a coupled hydrogeophysical inversion.
783 *Vadose Zone Journal*, 17(1), 0. doi: 10.2136/vzj2017.08.0154
- 784 LaBrecque, D. J., Heath, G., Sharpe, R., & Versteeg, R. (2004). Autonomous

- 785 Monitoring of Fluid Movement Using 3-D Electrical Resistivity Tomography.
786 *Journal of Environmental and Engineering Geophysics*, 9(3), 167–176. doi:
787 10.4133/JEEG9.3.167
- 788 Laloy, E., Javaux, M., Vanclooster, M., Roisin, C., & Biielders, C. L. (2011). Electrical
789 resistivity in a loamy soil: Identification of the appropriate pedo-electrical
790 model. *Vadose Zone Journal*, 10(3), 1023. doi: 10.2136/vzj2010.0095
- 791 Lehmann, P., Gambazzi, F., Suski, B., Baron, L., Askarinejad, A., Springman, S. M.,
792 ... Or, D. (2013). Evolution of soil wetting patterns preceding a hydrologically
793 induced landslide inferred from electrical resistivity survey and point measure-
794 ments of volumetric water content and pore water pressure. *Water Resources*
795 *Research*, 49(12), 7992–8004. doi: 10.1002/2013WR014560
- 796 Lesmes, D. P., & Friedman, S. P. (2005). Relationships between the electrical and
797 hydrogeological properties of rocks and soils. In Y. Rubin & S. S. Hubbard
798 (Eds.), *Hydrogeophysics* (pp. 87–128). Dordrecht: Springer Netherlands. doi:
799 10.1007/1-4020-3102-5_4
- 800 Linde, N., Binley, A., Tryggvason, A., Pedersen, L. B., & Revil, A. (2006). Improved
801 hydrogeophysical characterization using joint inversion of cross-hole electrical
802 resistance and ground-penetrating radar traveltime data. *Water Resources*
803 *Research*, 42(12), WR005131. doi: 10.1029/2006WR005131
- 804 Looms, M. C., Binley, A., Jensen, K. H., Nielsen, L., & Hansen, T. M. (2008).
805 Identifying unsaturated hydraulic parameters using an integrated data fusion
806 approach on cross-borehole geophysical data. *Vadose Zone Journal*, 7(1), 238.
807 doi: 10.2136/vzj2007.0087
- 808 Martini, E., Werban, U., Zacharias, S., Pohle, M., Dietrich, P., & Wollschläger, U.
809 (2017). Repeated electromagnetic induction measurements for mapping soil
810 moisture at the field scale: validation with data from a wireless soil moisture
811 monitoring network. *Hydrology and Earth System Sciences*, 21(1), 495–513.
812 doi: 10.5194/hess-21-495-2017
- 813 Michot, D., Benderitter, Y., Dorigny, A., Nicoullaud, B., King, D., & Tabbagh, A.
814 (2003). Spatial and temporal monitoring of soil water content with an irri-
815 gated corn crop cover using surface electrical resistivity tomography. *Water*
816 *Resources Research*, 39(5), 1–20. doi: 10.1029/2002WR001581
- 817 Miller, C. R., Routh, P. S., Brosten, T. R., & McNamara, J. P. (2008). Application
818 of time-lapse ERT imaging to watershed characterization. *Geophysics*, 73(3),
819 G7. doi: 10.1190/1.2907156
- 820 Oldenborger, G. A., & LeBlanc, A. M. (2015). Geophysical characterization of per-
821 mafrost terrain at Iqaluit International Airport, Nunavut. *Journal of Applied*
822 *Geophysics*, 123, 36–49. doi: 10.1016/j.jappgeo.2015.09.016
- 823 Ray, R. L., & Jacobs, J. M. (2007). Relationships among remotely sensed soil mois-
824 ture, precipitation and landslide events. *Natural Hazards*, 2(43), 211–222. doi:
825 10.1007/s11069-006-9095-9
- 826 Robinet, J., von Hebel, C., Govers, G., van der Kruk, J., Minella, J. P., Schlesner,
827 A., ... Vanderborght, J. (2018). Spatial variability of soil water content
828 and soil electrical conductivity across scales derived from electromagnetic
829 induction and time domain reflectometry. *Geoderma*, 314, 160–174. doi:
830 10.1016/j.geoderma.2017.10.045
- 831 Robinson, D. A., Lebron, I., Kocar, B., Phan, K., Sampson, M., Crook, N., &
832 Fendorf, S. (2009). Time-lapse geophysical imaging of soil moisture dynamics
833 in tropical deltaic soils: An aid to interpreting hydrological and geochemical
834 processes. *Water Resources Research*, 45(4). doi: 10.1029/2008WR006984
- 835 Scaini, A., Audebert, M., Hissler, C., Fencia, F., Gourdol, L., Pfister, L., & Beven,
836 K. J. (2017). Velocity and celerity dynamics at plot scale inferred from arti-
837 ficial tracing experiments and time-lapse ERT. *Journal of Hydrology*, 546,
838 28–43. doi: 10.1016/J.JHYDROL.2016.12.035
- 839 Schaap, M. G., Leij, F. J., & van Genuchten, M. T. (2001). Rosetta: A com-

- puter program for estimating soil hydraulic parameters with hierarchical pedotransfer functions. *Journal of Hydrology*, 251(3-4), 163–176. doi: 10.1016/S0022-1694(01)00466-8
- Scholer, M., Irving, J., Binley, A., & Holliger, K. (2011). Estimating vadose zone hydraulic properties using ground penetrating radar: The impact of prior information. *Water Resources Research*, 47(10), 1–14. doi: 10.1029/2011WR010409
- Shanahan, P. W., Binley, A., Whalley, W. R., & Watts, C. W. (2015). The use of electromagnetic induction to monitor changes in soil moisture profiles beneath different wheat genotypes. *Soil Science Society of America Journal*. doi: 10.2136/sssaj2014.09.0360
- Si, H. (2015). TetGen, a Delaunay-based quality tetrahedral mesh generator. *ACM Transactions on Mathematical Software*, 41(2), 1–36. doi: 10.1145/2629697
- Singha, K., Day-Lewis, F. D., Johnson, T., & Slater, L. D. (2014). Advances in interpretation of subsurface processes with time-lapse electrical imaging. *Hydrological Processes*, 29(6), 1549–1576. doi: 10.1002/hyp.10280
- Taylor, J. R. (1982). *An Introduction to Error Analysis: The Study of Uncertainties in Physical Measurements*. University Science Books.
- Tso, C.-H. M., Kuras, O., Wilkinson, P. B., Uhlemann, S., Chambers, J. E., Meldrum, P. I., ... Binley, A. (2017). Improved characterisation and modelling of measurement errors in electrical resistivity tomography (ERT) surveys. *Journal of Applied Geophysics*, 146, 103–119. doi: 10.1016/J.JAPPGEO.2017.09.009
- Turkeltaub, T., Jia, X., Zhu, Y., Shao, M.-A., & Binley, A. (2018). Recharge and nitrate transport through the deep vadose zone of the Loess Plateau: A regional-scale model investigation. *Water Resources Research*, 54(7), 4332–4346. doi: 10.1029/2017WR022190
- Uhlemann, S., Chambers, J., Wilkinson, P., Maurer, H., Merritt, A., Meldrum, P., ... Dijkstra, T. (2017). Four-dimensional imaging of moisture dynamics during landslide reactivation. *Journal of Geophysical Research: Earth Surface*, 122(1), 398–418. doi: 10.1002/2016JF003983
- Uhlemann, S., Sorensen, J. P. R., House, A. R., Wilkinson, P. B., Roberts, C., & Goody, D. C. (2016). Integrated time-lapse geoelectrical imaging of wetland hydrological processes. *Water Resources Research*, 52(3), 1607–1625. doi: 10.1002/2015WR017932
- von Hebel, C., Rudolph, S., Mester, A., Huisman, J. A., Kumbhar, P., Vereecken, H., & van der Kruk, J. (2014). Three-dimensional imaging of subsurface structural patterns using quantitative large-scale multiconfiguration electromagnetic induction data. *Water Resources Research*, 50(3), 2732–2748. doi: 10.1002/2013WR014864
- Wehrer, M., & Slater, L. D. (2015). Characterization of water content dynamics and tracer breakthrough by 3-D electrical resistivity tomography (ERT) under transient unsaturated conditions. *Water Resources Research*, 51(1), 97–124. doi: 10.1002/2014WR016131
- Weller, A., Slater, L., & Nordsiek, S. (2013). On the relationship between induced polarization and surface conductivity: Implications for petrophysical interpretation of electrical measurements. *Geophysics*, 78(5), D315–D325. doi: 10.1190/geo2013-0076.1
- Whalley, W. R., Binley, A., Watts, C. W., Shanahan, P., Dodd, I. C., Ober, E. S., ... Hawkesford, M. J. (2017). Methods to estimate changes in soil water for phenotyping root activity in the field. *Plant and Soil*, 415(1-2), 407–422. doi: 10.1007/s11104-016-3161-1
- Wiese, B. U., Wagner, F. M., Norden, B., Maurer, H., & Schmidt-Hattenberger, C. (2018). Fully coupled inversion on a multi-physical reservoir model Part I: Theory and concept. *International Journal of Greenhouse Gas Control*, 75, 262–272. doi: 10.1016/J.IJGGC.2018.05.013

895
896
897
898
899
900
901
902
903
904
905
906
907
908
909

- Winship, P., Binley, A., & Gomez, D. (2006). Flow and transport in the unsaturated Sherwood Sandstone: characterization using cross-borehole geophysical methods. *Geological Society, London, Special Publications*, 263(1), 219–231. doi: 10.1144/GSL.SP.2006.263.01.12
- Yamakawa, Y., Kosugi, K., Katsura, S., Masaoka, N., & Mizuyama, T. (2012). Spatial and temporal monitoring of water content in weathered granitic bedrock using electrical resistivity imaging. *Vadose Zone Journal*, 11(1), 0. doi: 10.2136/vzj2011.0029
- Zhang, Y., Schaap, M., Guadagnini, A., & Neuman, S. (2016). Inverse modeling of unsaturated flow using clusters of soil texture and pedotransfer functions. *Water Resources Research*, 52(10), 1–45. doi: 10.1002/2016WR019016
- Zhu, P., Shi, L., Zhu, Y., Zhang, Q., Huang, K., & Williams, M. (2017). Data assimilation of soil water flow via ensemble Kalman filter: Infusing soil moisture data at different scales. *Journal of Hydrology*, 555, 912–925. doi: 10.1016/j.jhydrol.2017.10.078

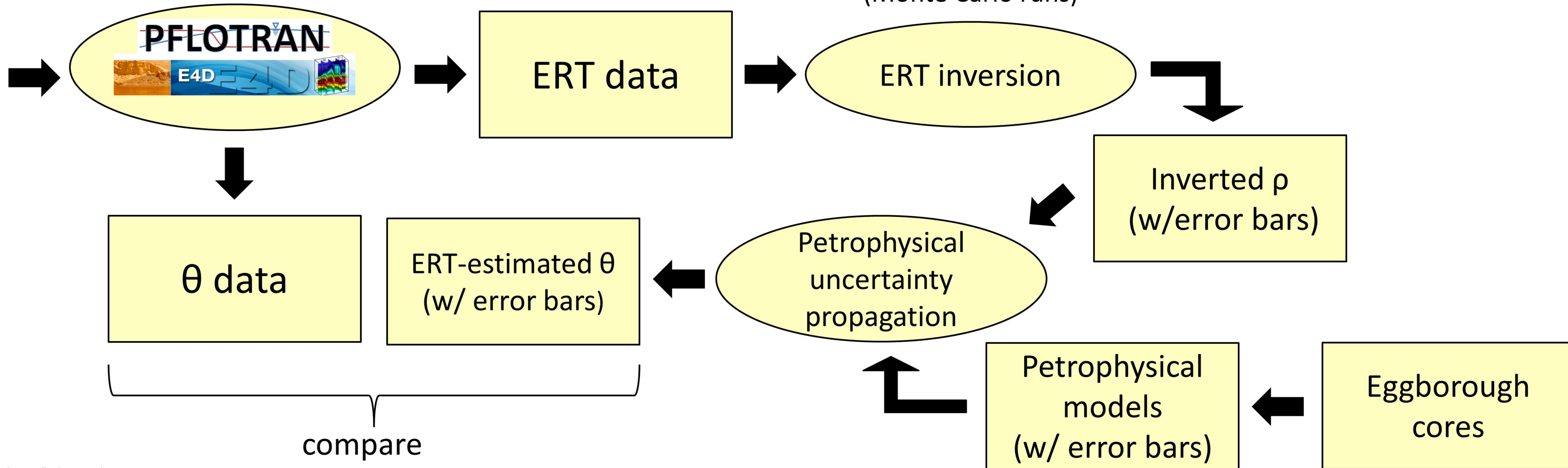
Accepted Article

Figure 1.

Accepted Article

Coupled hydrogeophysical simulation
using PFLOTRAN-E4D

Difference inversion of ERT data
(Monte Carlo runs)



Accepted Article

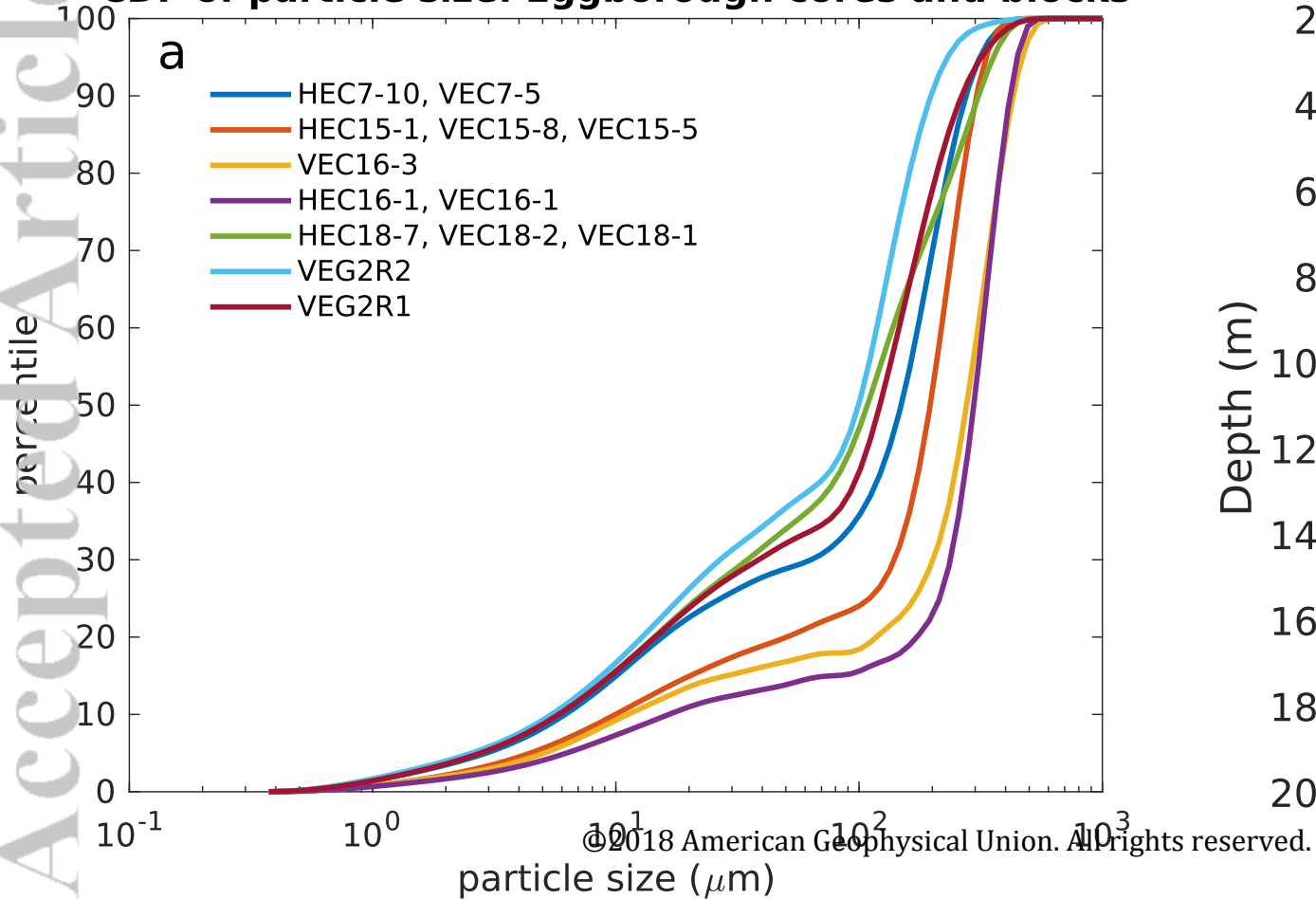
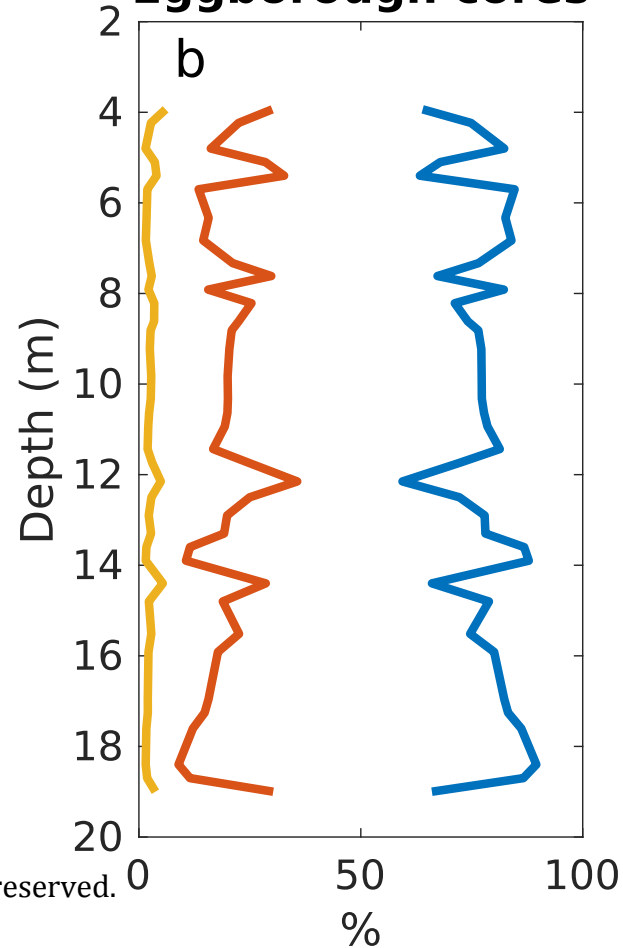
CDF of particle size: Eggborough cores and blocks**Eggborough cores**

Figure 3.

Accepted Article

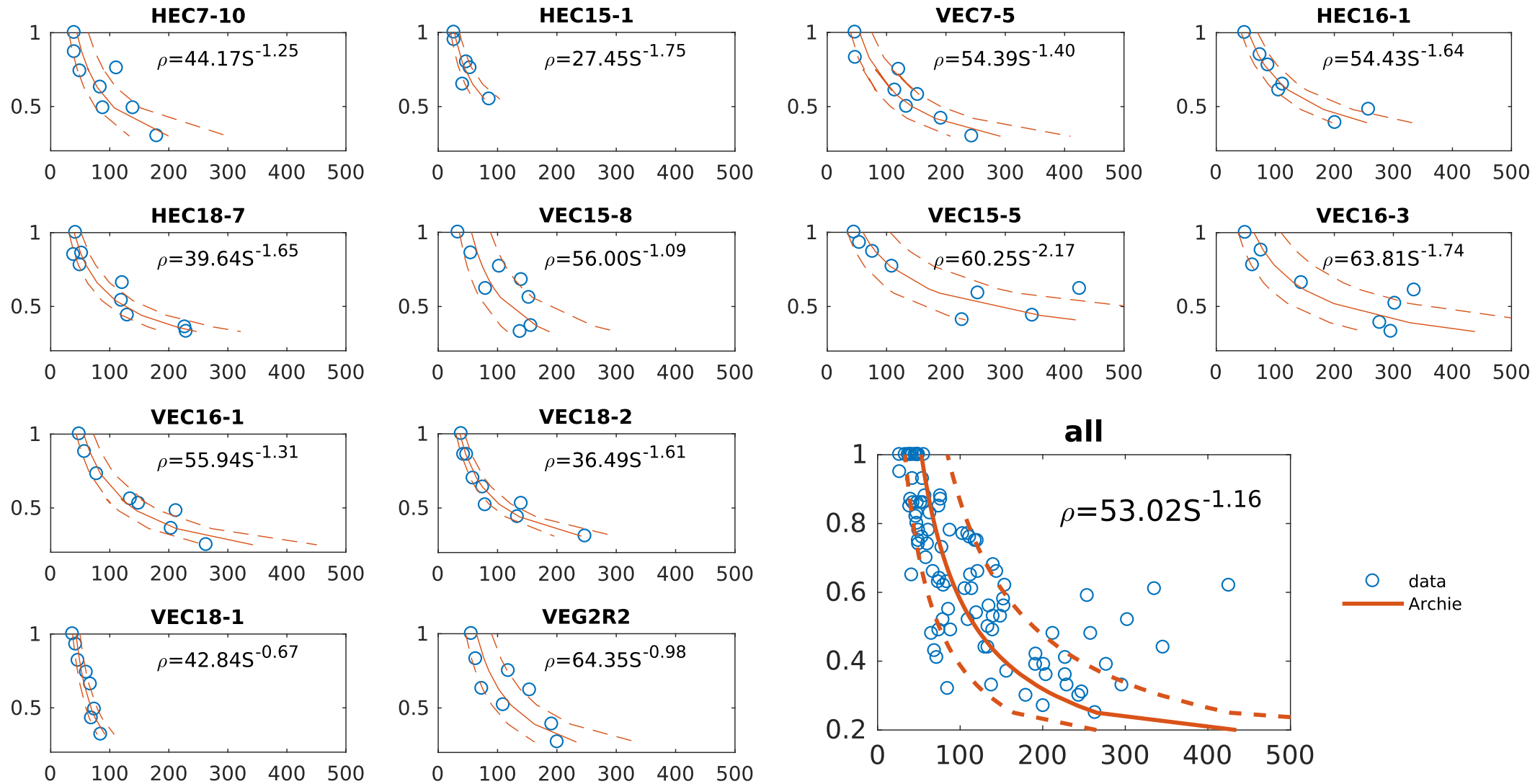
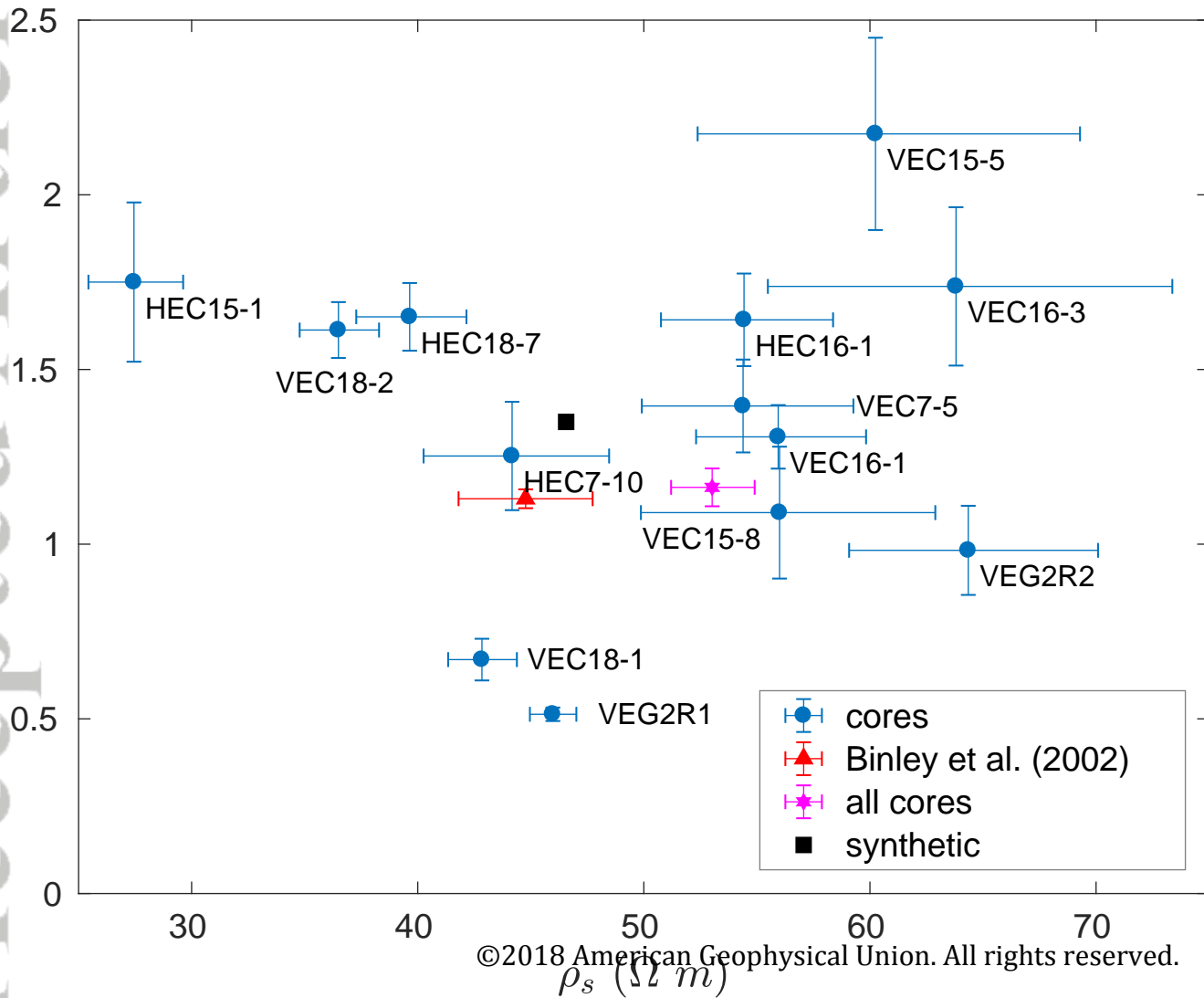
water saturation S 

Figure 4.

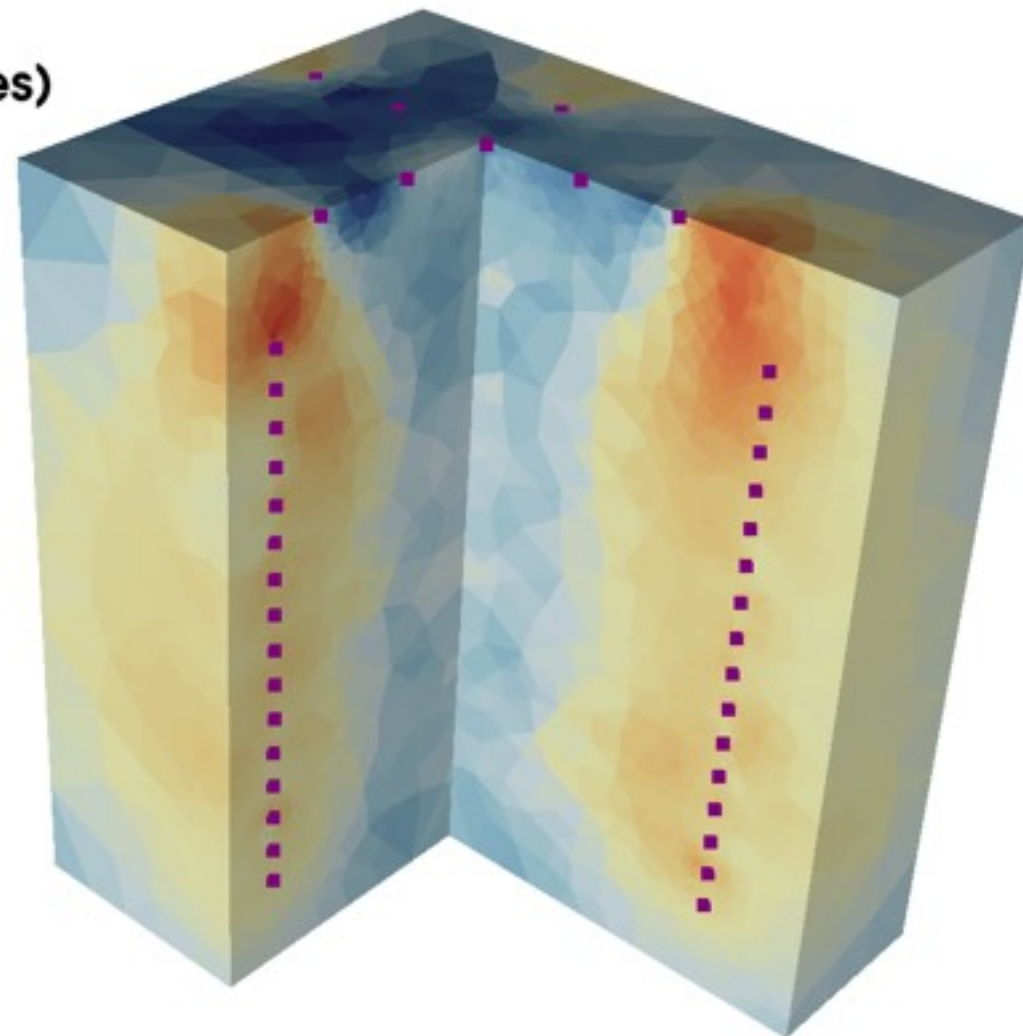
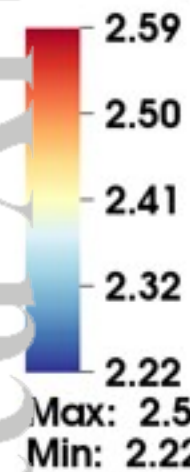
Accepted Article



Accepted Article

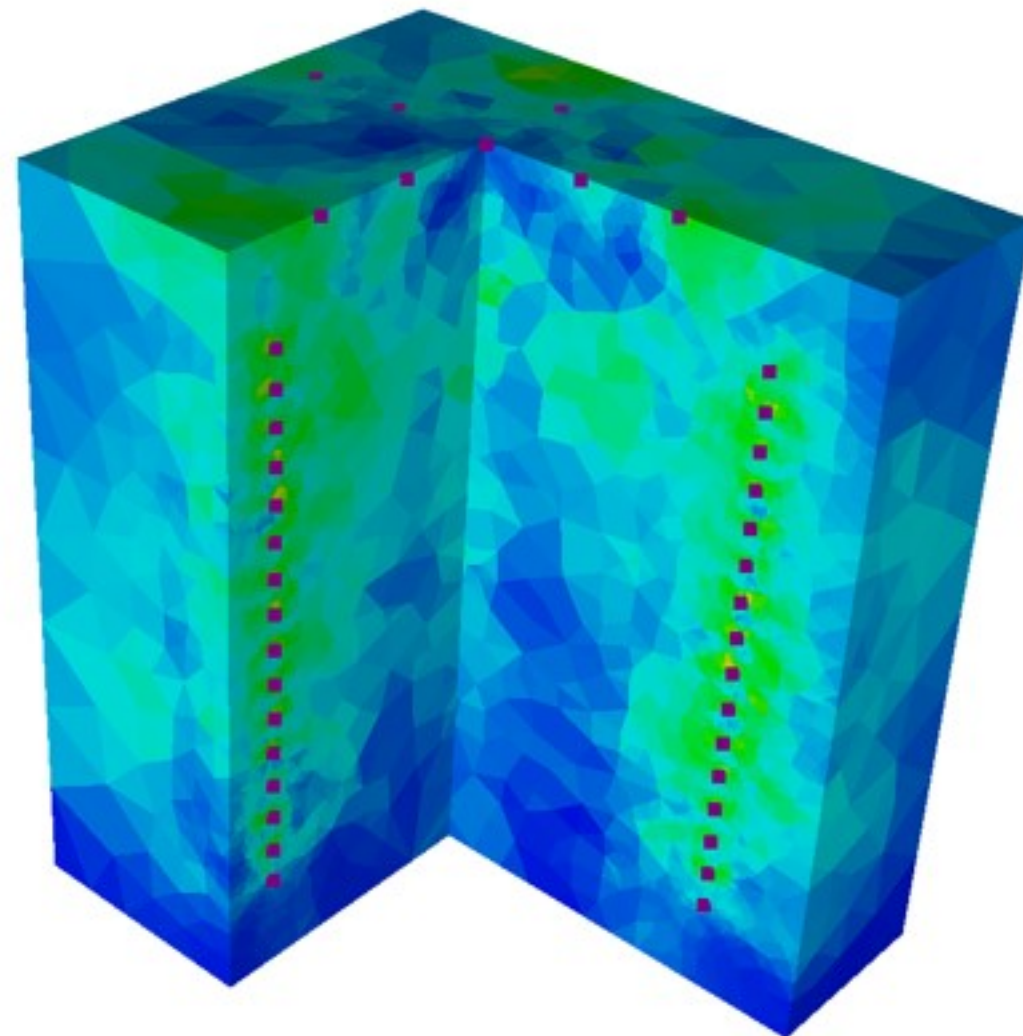
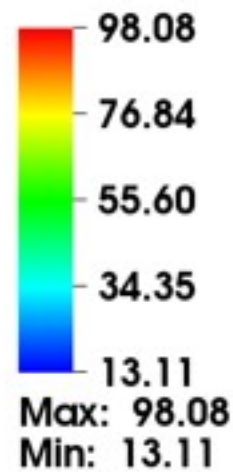
a

mean log(res)

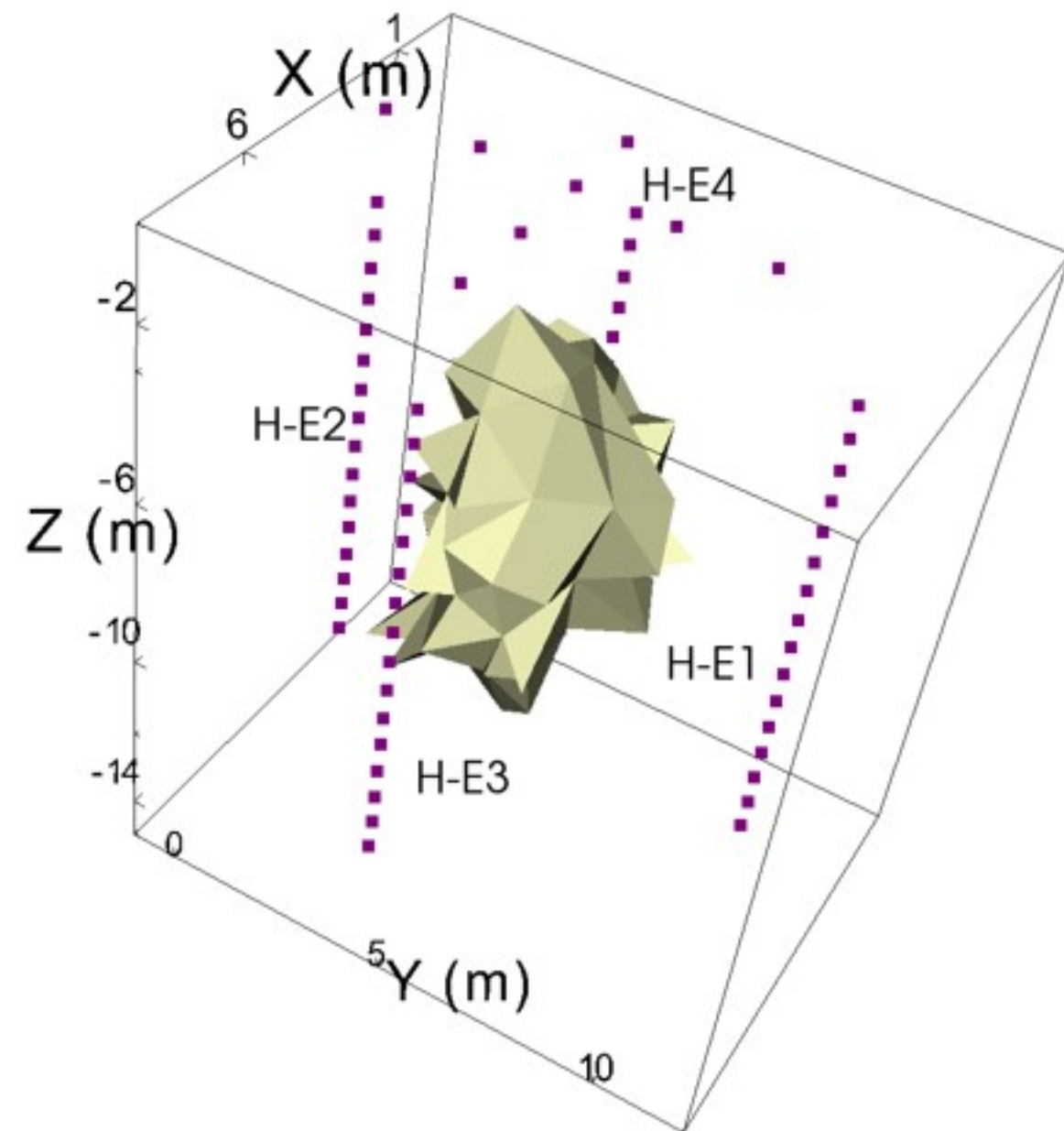


b

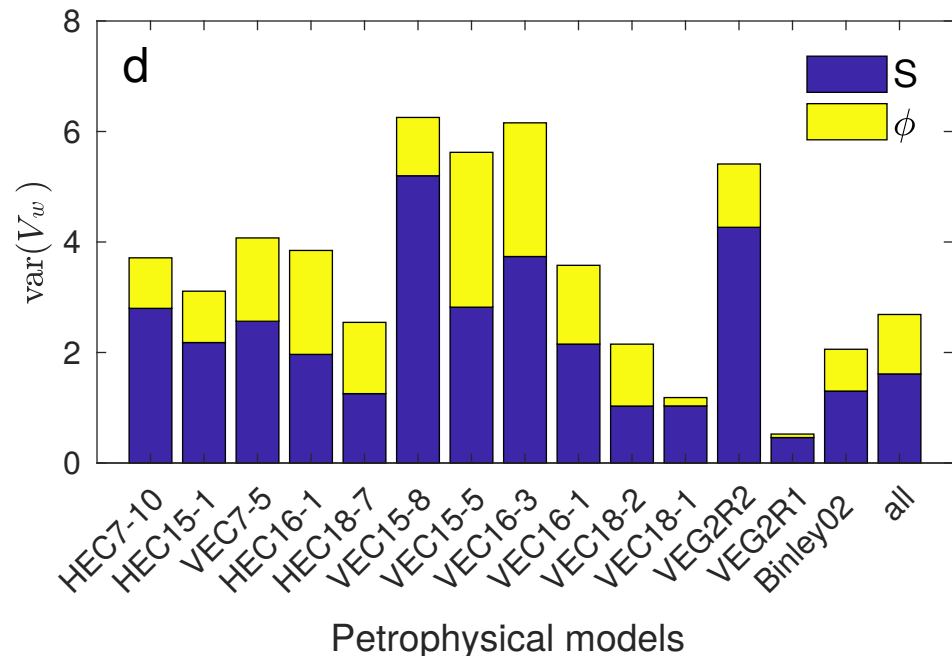
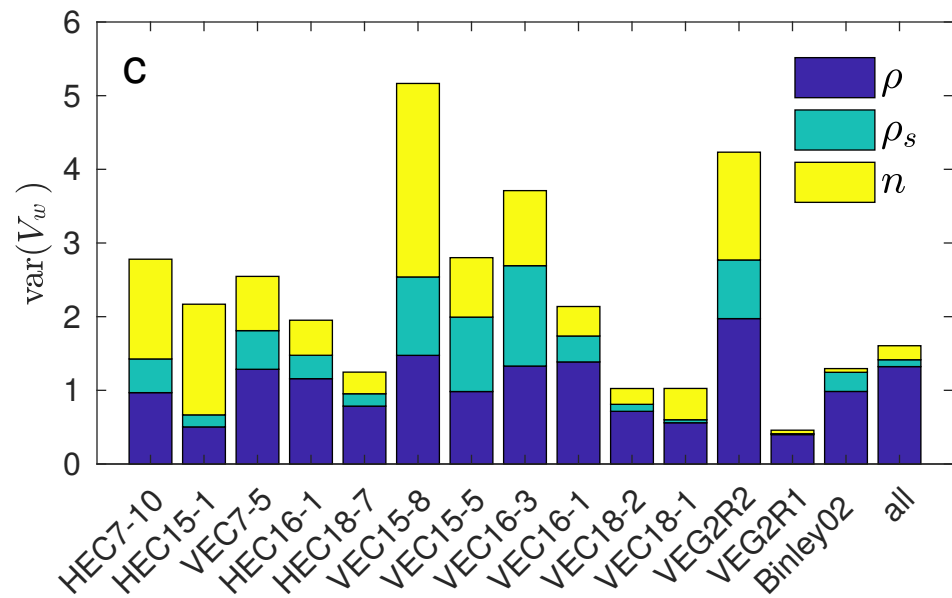
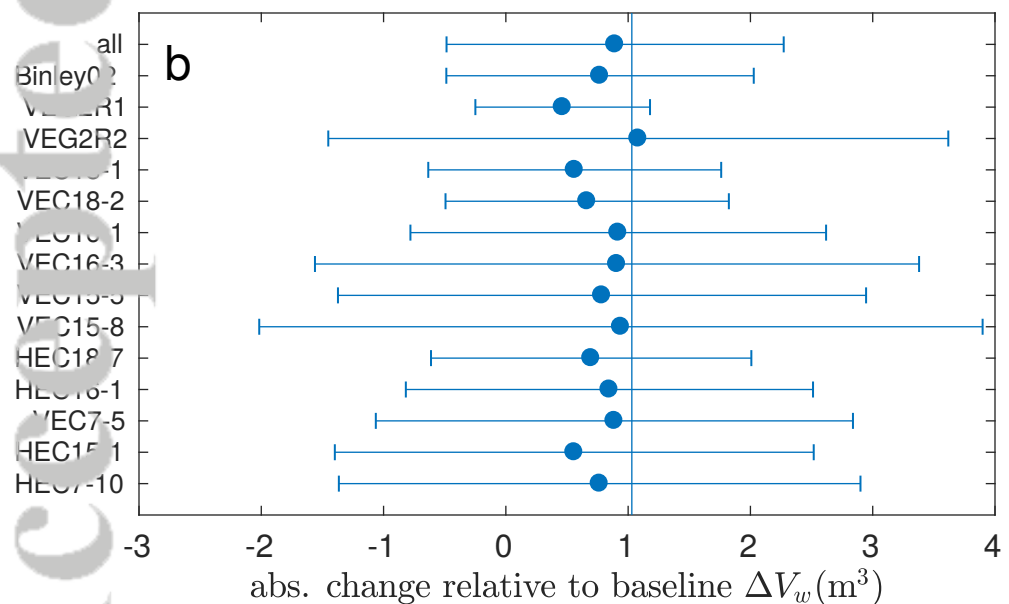
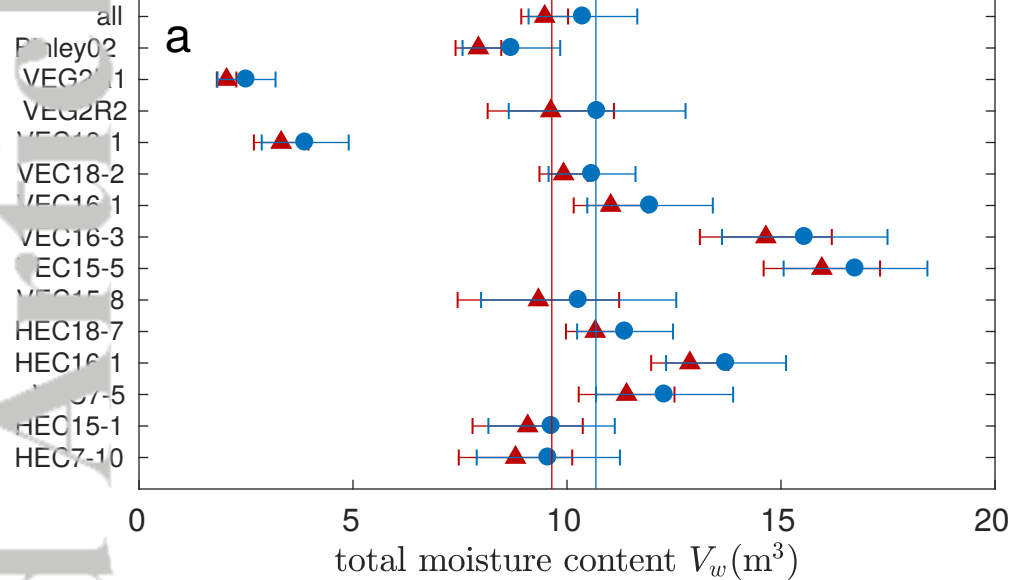
std(res)



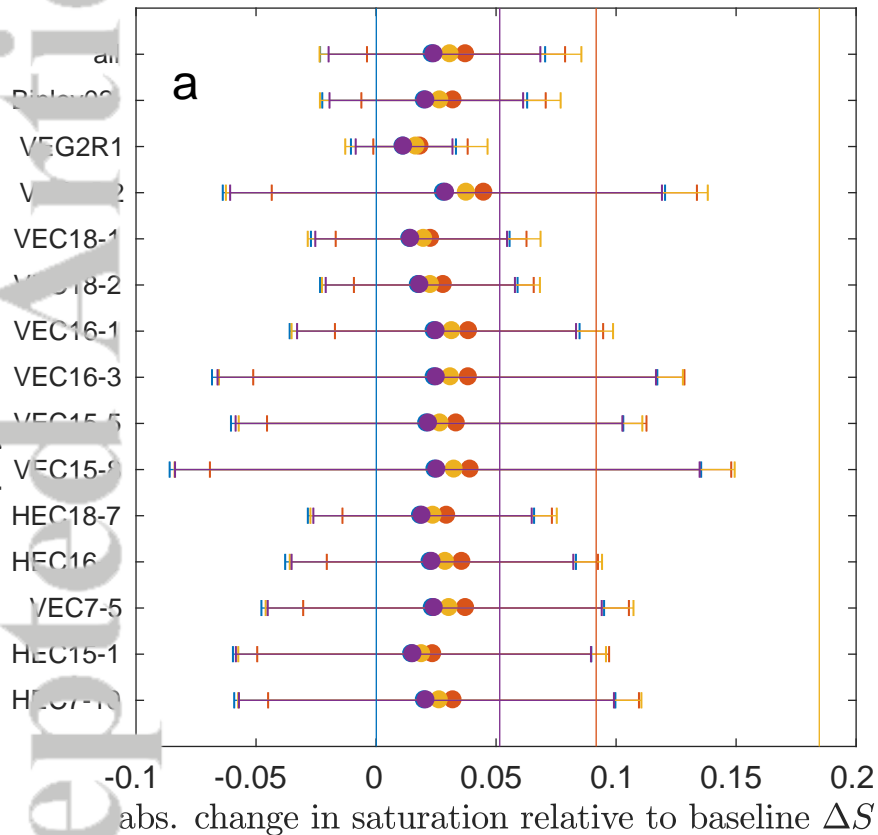
c



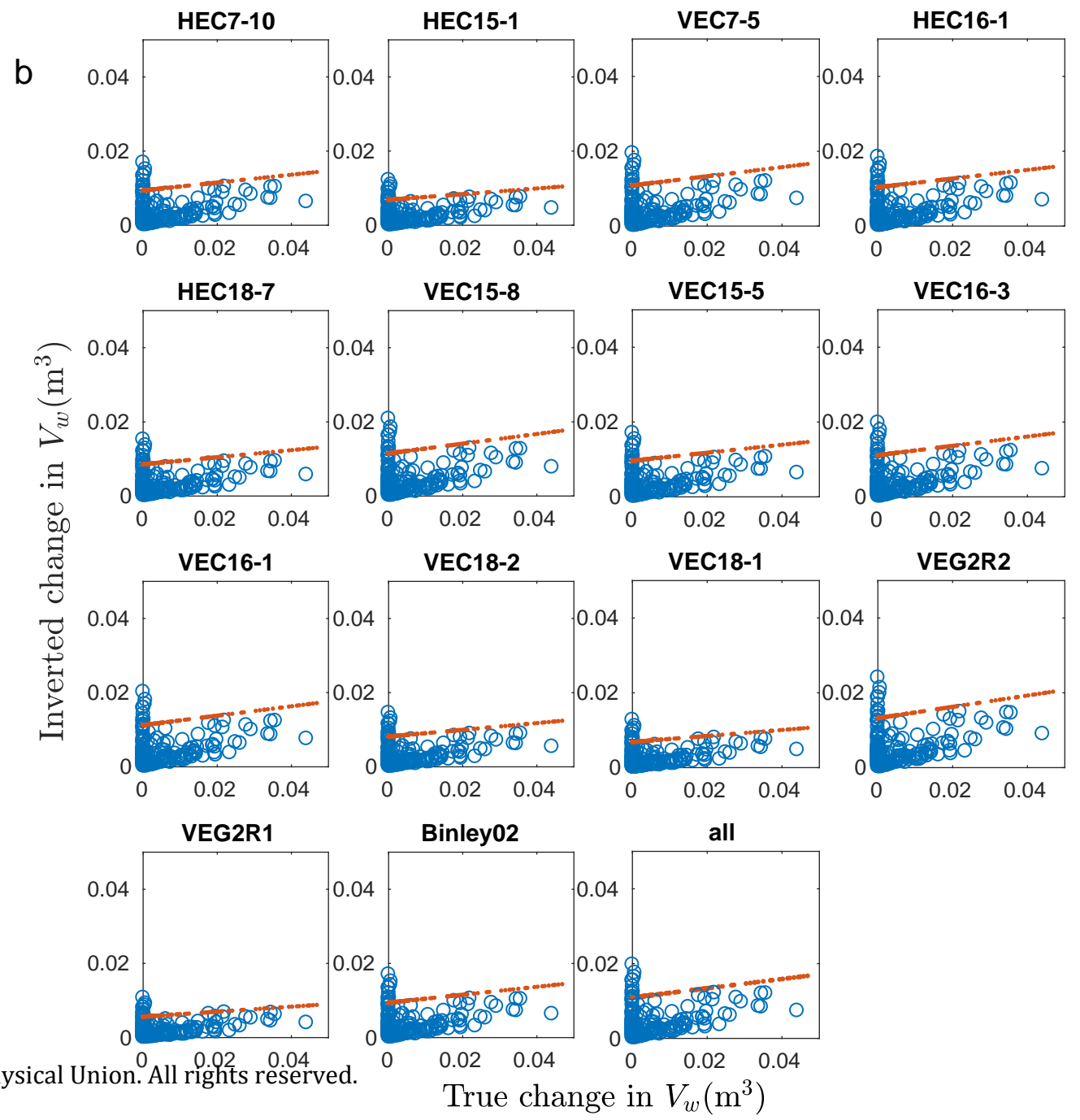
Accepted Article

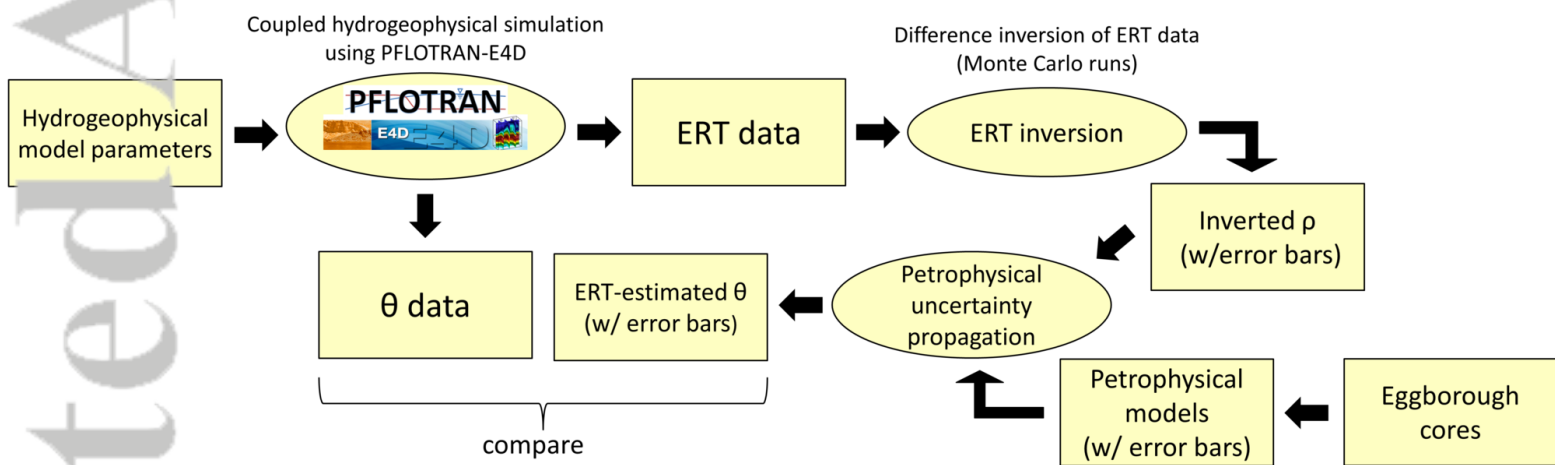


Accepted Article

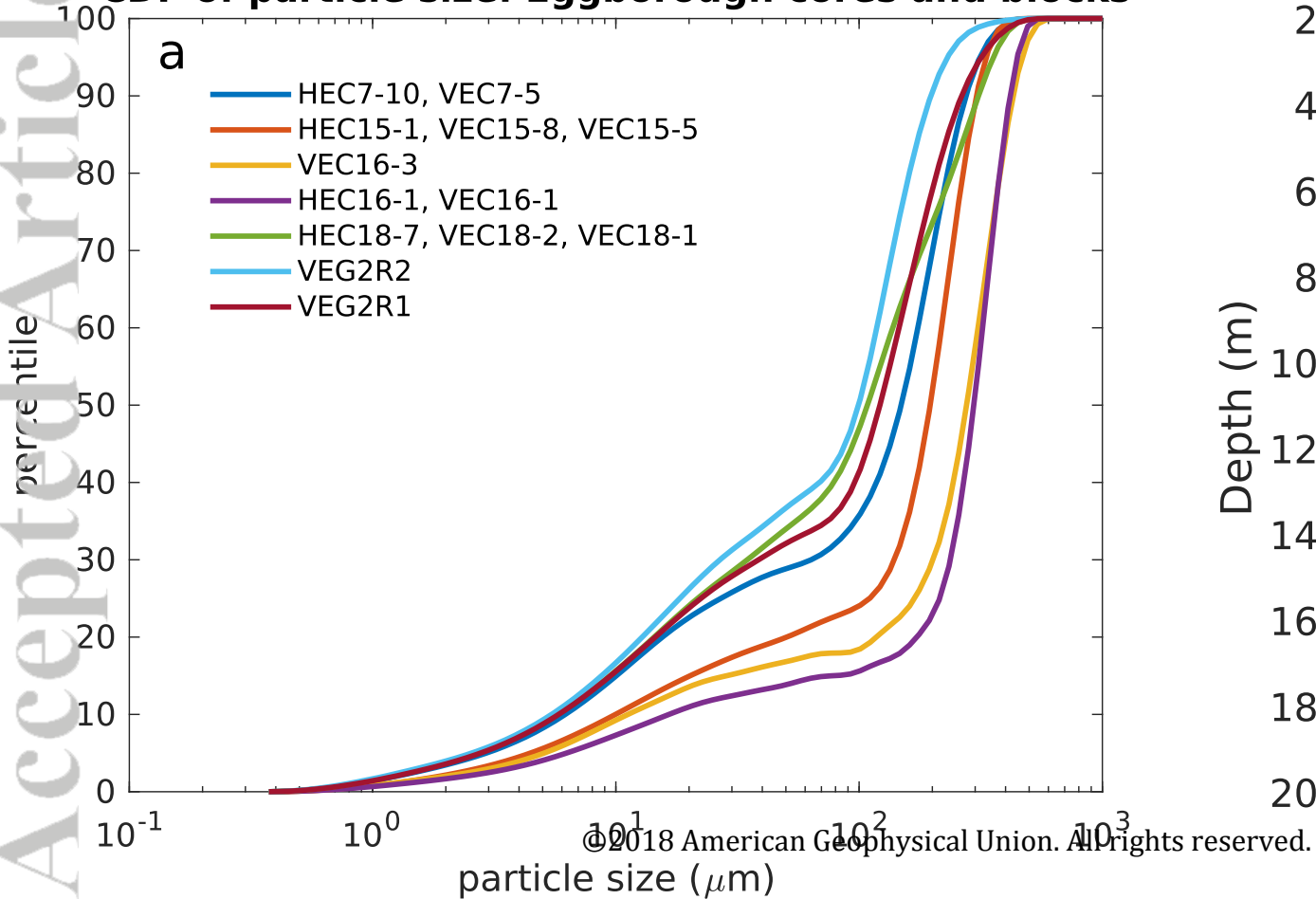
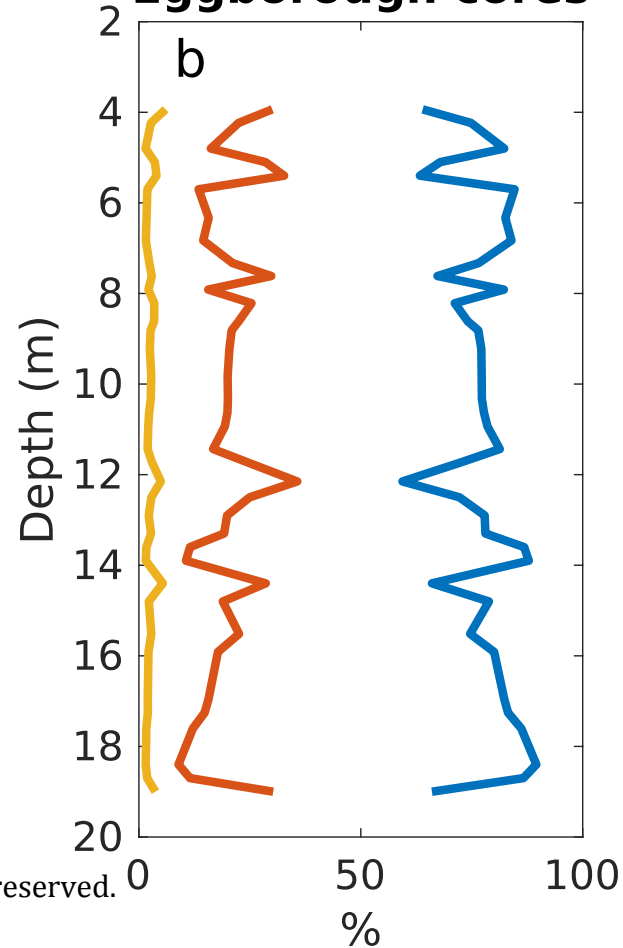


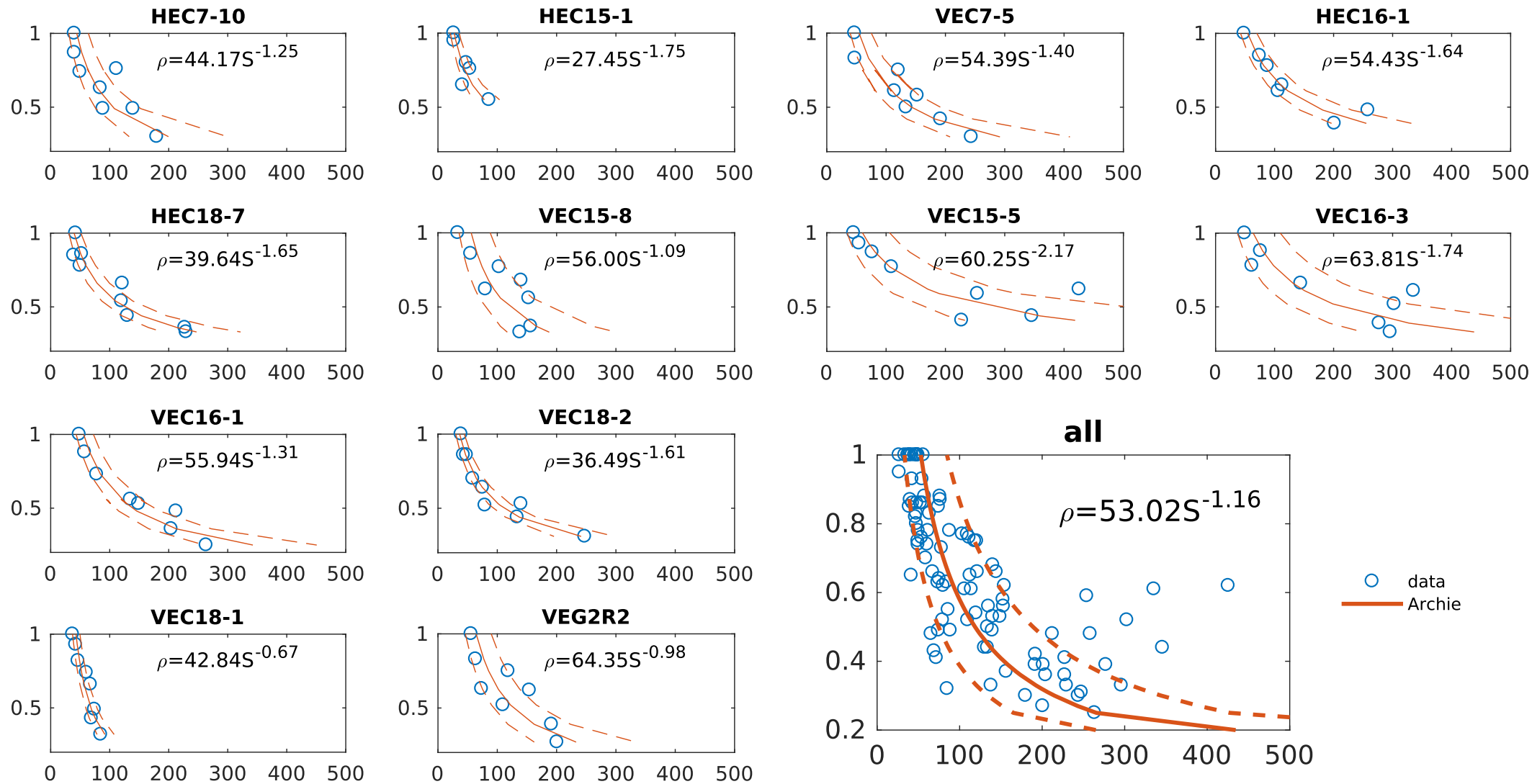
- cell centroid: [4.01, 2.80, -8.52]
- cell centroid: [2.14, 4.96, -6.26]
- cell centroid: [3.20, 4.13, -9.54]
- cell centroid: [1.65, 3.29, -5.61]

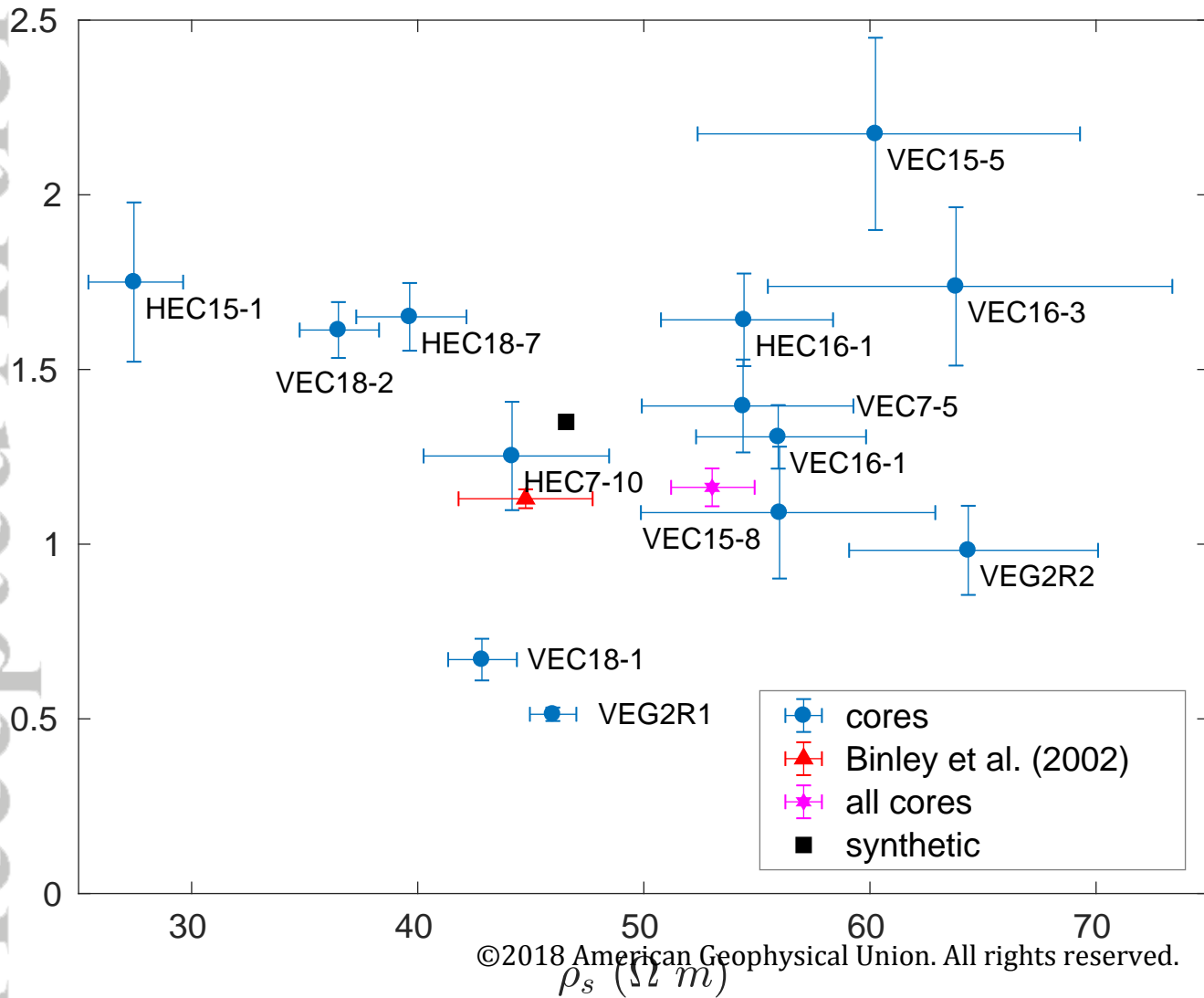


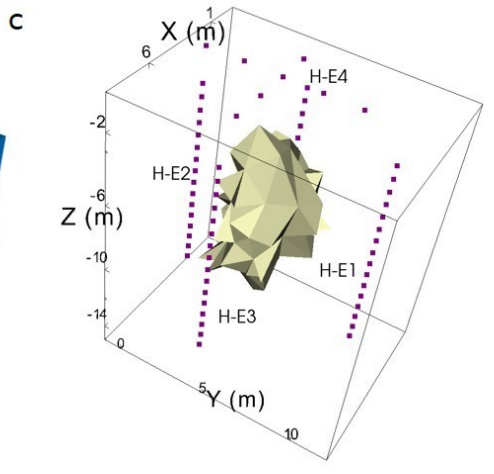
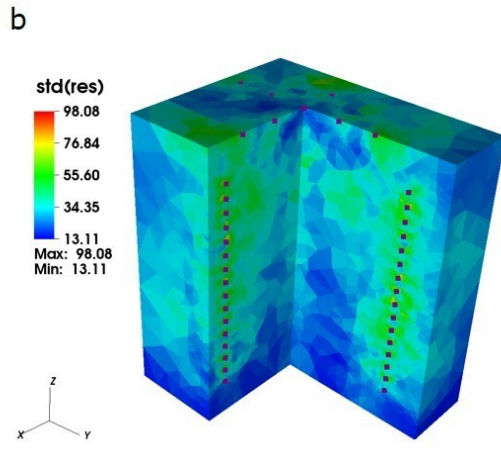
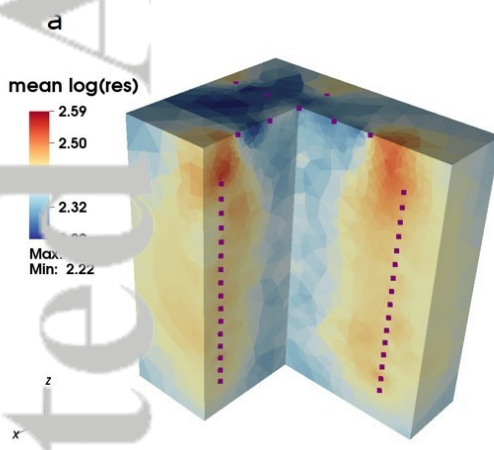


2019WR024964-f01-z-.png

CDF of particle size: Eggborough cores and blocks**Eggborough cores**

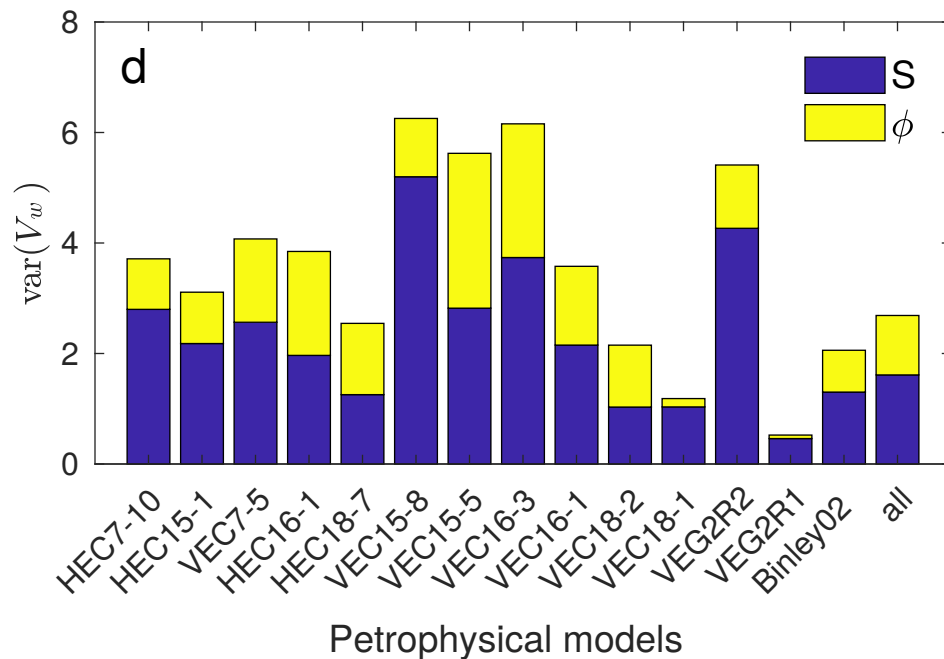
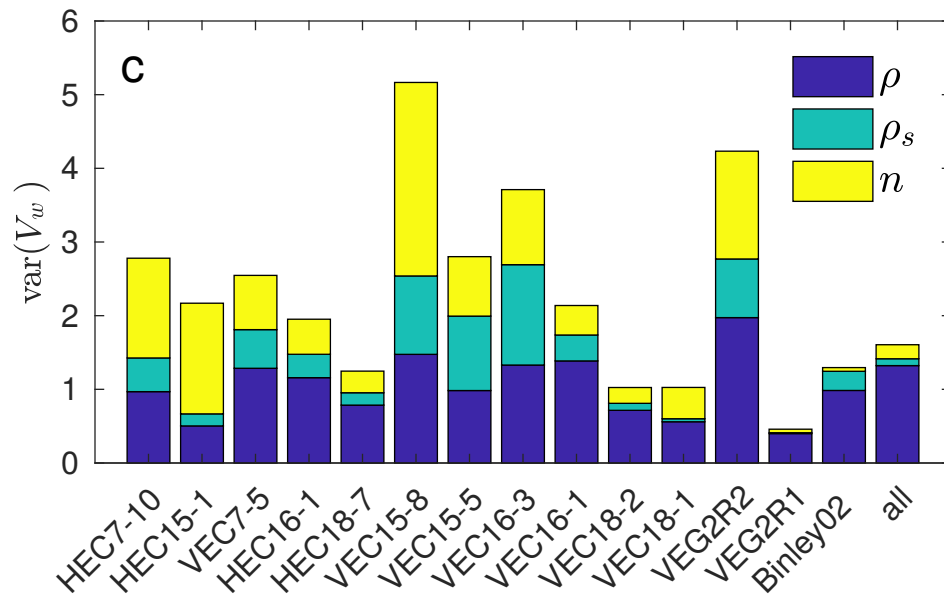
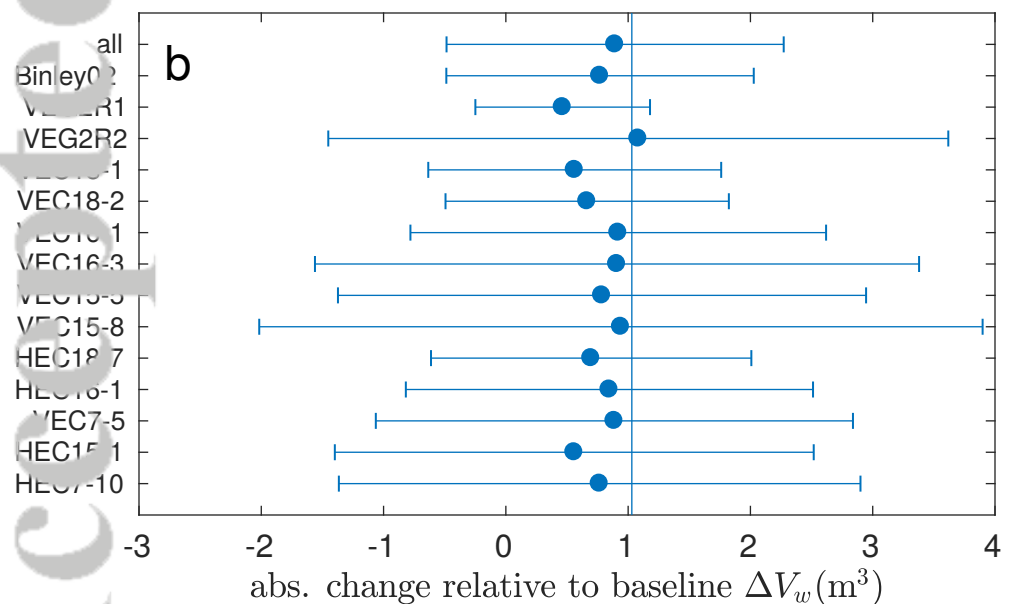
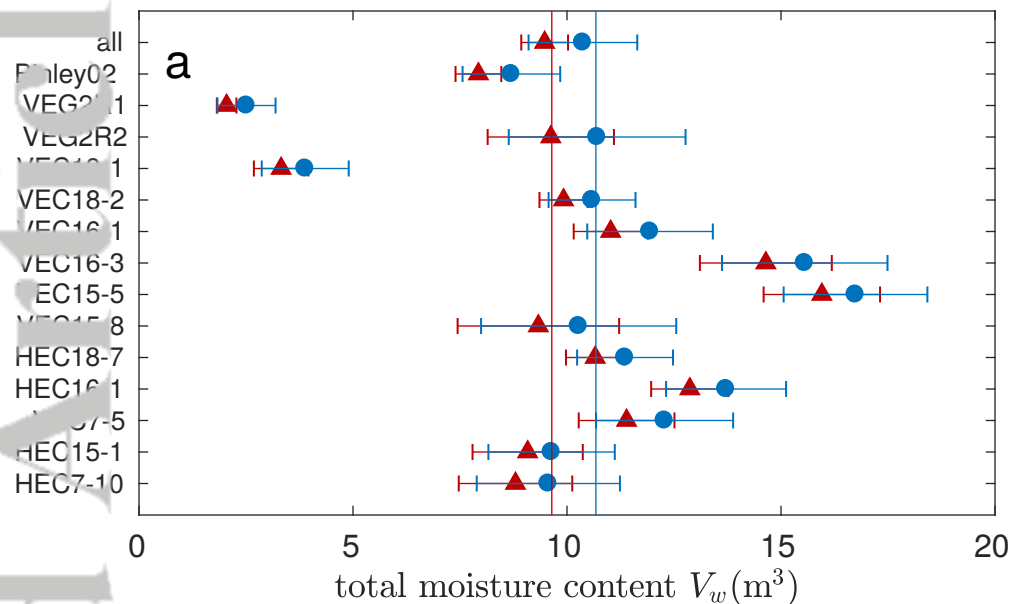
water saturation S 

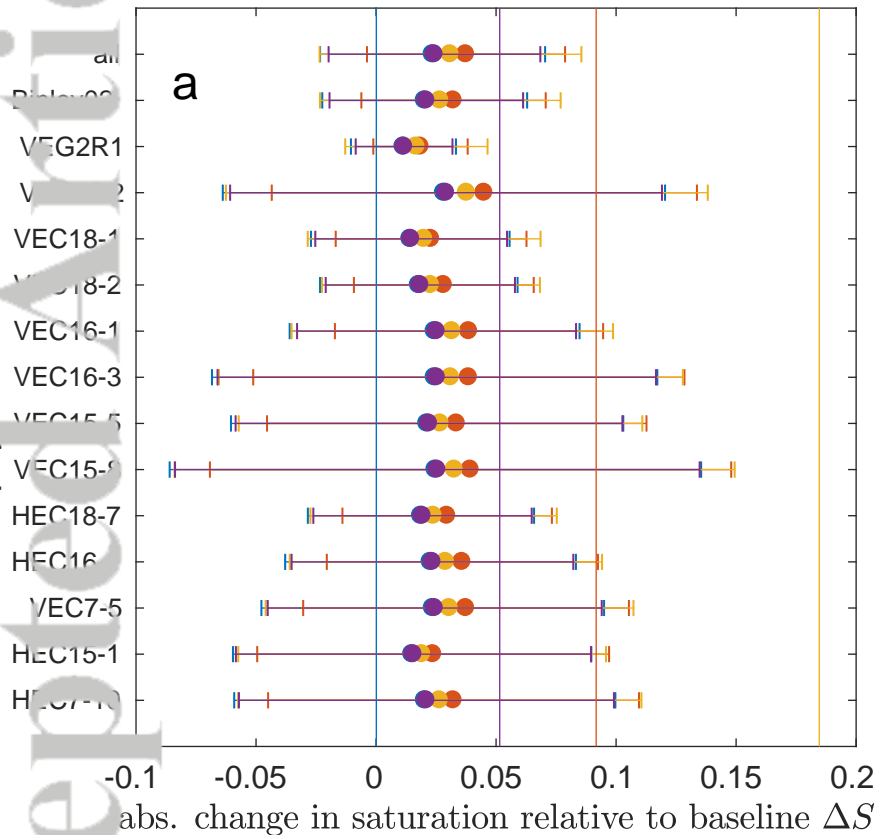
n 



2019WR024964-f05-z-.jpg

Day 7 (Pre-injection) Day 18 (Post-injection)





- cell centroid: [4.01, 2.80, -8.52]
- cell centroid: [2.14, 4.96, -6.26]
- cell centroid: [3.20, 4.13, -9.54]
- cell centroid: [1.65, 3.29, -5.61]

